

**A multi-layered and dynamic apical extracellular matrix
shapes the vulva lumen in *Caenorhabditis elegans***

Jennifer D. Cohen¹, Alessandro P. Sparacio¹, Alexandra C. Belfi¹, Rachel Forman-
Rubinsky¹, David H. Hall², Hannah M. Maul-Newby³, Alison R. Frand³, and Meera V.
Sundaram^{1,4}

¹ Department of Genetics, University of Pennsylvania Perelman School of Medicine

² Department of Neuroscience, Albert Einstein College of Medicine

³ Department of Biological Chemistry, David Geffen School of Medicine, University of
California, Los Angeles

⁴ Author for Correspondence

415 Curie Blvd, Philadelphia PA 19104-6145

sundaram@pennmedicine.upenn.edu

(215) 573-4527

Abstract

Biological tubes must develop and maintain their proper diameter in order to transport materials efficiently. These tubes are molded and protected in part by apical extracellular matrices (aECMs) that line their lumens. Despite their importance, aECMs are difficult to image in vivo and therefore poorly understood. The *C. elegans* vulva has been a paradigm for understanding many aspects of organogenesis. Here we describe the vulva luminal matrix, which contains chondroitin proteoglycans, Zona Pellucida (ZP) domain proteins, and other glycoproteins and lipid transporters related to those in mammals. Confocal and transmission electron microscopy revealed, with unprecedented detail, a complex and dynamic aECM. Different matrix factors assemble on the apical surfaces of each vulva cell type, with clear distinctions seen between Ras-dependent (1°) and Notch-dependent (2°) cell types. Genetic perturbations suggest that chondroitin and other aECM factors together generate a structured scaffold that both expands and constricts lumen shape.

Introduction

During tubulogenesis, lumen formation and expansion generally occur in the context of fluid influx and/or apical extracellular matrix (aECM) secretion (reviewed by (Luschnig & Uv, 2014; Navis & Nelson, 2016)). Tubular epithelia drive water into the lumen by establishing ionic and osmotic gradients using various ion pumps and channels; the resulting hydrostatic pressure can stimulate lumen enlargement (Bagnat, Cheung, Mostov, & Stainier, 2007; Dong, Deng, & Jiang, 2011; Khan et al., 2013; Kolotuev, Hyenne, Schwab, Rodriguez, & Labouesse, 2013; Navis, Marjoram, & Bagnat, 2013). But ions and water are not the only molecules being secreted into nascent lumens; proteoglycans, lipids, mucins, zona pellucida (ZP) domain proteins, and/or other matrix factors are also present and can contribute to lumen shaping (Devine et al., 2005; Gill et al., 2016; Hwang, Olson, Esko, & Horvitz, 2003; Jazwinska, Ribeiro, & Affolter, 2003; Lane, Koehl, Wilt, & Keller, 1993; Rosa, Metzstein, & Ghabrial, 2018; Strilić et al., 2009; Tønning et al., 2005). These aECM factors may act like sponges to bind and organize water molecules and generate outward pushing forces (Lane et al., 1993; Syed et al., 2012), or they may assemble into fibrils or other specialized structures to exert more localized pushing or pulling forces on tube membranes (Andrew & Ewald, 2010; Linde-Medina & Marcucio, 2018; Luschnig & Uv, 2014; Plaza, Chanut-Delalande, Fernandes, Wassarman, & Payre, 2010). aECMs may also bind and present or sequester various signaling molecules that impact cell identity or behavior (Judge & Dietz, 2005; Perrimon & Bernfield, 2000). aECMs of varying types are present in all tubular epithelia; examples in mammals include the vascular glycocalyx, lung surfactant and the mucin-rich linings of the gastrointestinal tract and upper airway (Bernhard, 2016; Johansson, Sjövall, & Hansson, 2013; Webster & Tarran, 2018). However, such aECMs generally appear translucent by light microscopy and are easily destroyed by standard chemical fixation protocols, and thus the organizational structures and lumen-shaping mechanisms of most luminal matrices remain poorly understood.

65

66 Vulva development in the nematode *Caenorhabditis elegans* has been a paradigm for
67 understanding many aspects of cell fate specification and organogenesis (Schindler &
68 Sherwood, 2013; Schmid & Hajnal, 2015). The vulva tube consists of twenty-two cells of seven
69 different cell types, organized as seven stacked toroids (vulA, vulB1, vulB2, vulC, vulD, vulE and
70 vulF) (Sharma-Kishore, White, Southgate, & Podbilewicz, 1999) (Figure 1). In adult
71 hermaphrodites, the vulva connects to the uterus and serves as a passageway to allow sperm
72 entry and the release of fertilized eggs. In the 40+ years since vulva cell lineages were first
73 described (Sulston & Horvitz, 1977), much has been learned about how different vulva cell fates
74 are specified and how they arrange to form the tube structure. It is known that the
75 glycosaminoglycan (GAG) chondroitin promotes initial expansion of the vulva lumen during
76 morphogenesis (Hwang, Olson, Brown, Esko, & Horvitz, 2003), the lumen changes shape and
77 eventually narrows, and then later, in the adult, collagenous cuticle lines the functional vulva
78 tube (Page & Johnstone, 2007; Sulston & Horvitz, 1977). However, the specific contents,
79 organization, and morphogenetic roles of the luminal matrix within the developing vulva have
80 remained, for the most part, uncharacterized.

81

82 Here we show that a spatially and temporally dynamic aECM assembles and
83 disassembles within the vulva lumen during morphogenesis. This transient aECM shares
84 components with the glycocalyx-like sheath or pre-cuticle matrix that coats other apical surfaces
85 in *C. elegans* prior to each round of cuticle secretion (Forman-Rubinsky, Cohen, & Sundaram,
86 2017; Gill et al., 2016; Katz, Maybrun, Maul-Newby, & Frand, 2018; Kelley et al., 2015;
87 Labouesse, 2012; Lazetic & Fay, 2017; Mancuso et al., 2012; Priess & Hirsh, 1986; Vuong-
88 Brender, Suman, & Labouesse, 2017). It contains both fibrillar and granular components, and

also extracellular vesicles, as observed at the ultrastructural level. Different combinations of matrix factors assemble on the apical surfaces of each of the seven different vulva cell types, with particularly clear distinctions seen between Ras-dependent (1°) and Notch-dependent (2°) cell types. Genetic perturbation experiments suggest that chondroitin and other aECM factors together generate a structured scaffold that has both lumen expanding and lumen constraining roles.

Results

Background: vulva tube formation

Specification and generation of the seven vulva cell types occurs during the L2 and L3 larval stages, while toroid formation and other aspects of tube morphogenesis occur during the L4 stage (Figures 1 and 2). The twenty-two cells of the vulva derive from three of six total possible vulva precursor cells (VPCs), named P3.p-P8.p. Signaling by the Epidermal Growth Factor Receptor (EGFR)-Ras-ERK and Notch pathways specifies one central 1° and two flanking 2° VPC fates (Figure 1B) (Schmid & Hajnal, 2015; Sternberg & Horvitz, 1989). First, an EGF-like signal from the gonadal anchor cell (AC) induces P6.p to adopt the 1° VPC fate, and that cell then expresses Delta/Serrate/LAG-2 (DSL)-like ligands to induce its neighbors, P5.p and P7.p, to adopt the 2° cell fate. The 1° VPC (P6.p) divides to generate eight descendants: 4 vulF and 4 vulE cells. The 2° VPCs (P5.p and P7.p) divide to generate seven descendants each: 1 vulD, 2 vulC, 1 vulB2, 1 vulB1 and 2 vulA cells. Primary descendants produce an unknown cue that promotes basement membrane invasion by the gonadal AC, which is the first step in forming a vulva-uterine connection (Ihara et al., 2011; Matus et al., 2014; Sherwood & Sternberg, 2003). As they divide, 1° descendants detach from the underlying epidermal cuticle and move dorsally, and also detach from the overlying basement membrane to allow further AC penetration (Ihara et al., 2011; Matus et al., 2014; McClatchey et al., 2016). Upon completion of

vulva cell divisions, 2° descendants migrate inward in a Rac and Rho-dependent manner, and push the more central 2° descendants and the 1° descendants further dorsally to generate the vulva invagination seen at early L4 (Farooqui et al., 2012; Kishore & Sundaram, 2002; Sharma-Kishore et al., 1999; Shemer, Kishore, & Podbilewicz, 2000). As cells of the same type meet, they eventually fuse to form the seven vulva toroids (Sharma-Kishore et al., 1999).

Ten different stages of L4 vulva morphogenesis (L4.0-L4.9) have been distinguished based on changing lumen morphology, as observed by differential interference contrast (DIC) microscopy (Mok, Sternberg, & Inoue, 2015). To visualize cell shapes that correspond to each of these stages, we used the RhoG marker MIG-2::GFP (Honigberg & Kenyon, 2000) to label all vulva cell membranes (Figures 1D, 2). At L4.0, the vulva invagination is very narrow, but it enlarges to approximately 10 microns in diameter by the L4.3 stage. Between L4.3 and L4.4, the uterine lumen and the dorsal-most part of the vulva lumen both expand (Ihara et al., 2011; Matus et al., 2014), and the gonadal AC fuses with the uterine seam (utse), leaving just a thin part of its membrane as a hymen separating the two lumens (Sapir et al., 2007; Sharma-Kishore et al., 1999). The vulB1 and vulB2 cells also develop increasingly concave apical surfaces, creating a “Christmas tree-like” lumen appearance at L4.4-L4.5, and a more “cactus-like” appearance by L4.7. In the final morphogenetic stages, collectively termed eversion, further cell shape changes and rearrangements occur to narrow the lumen and generate the closed lips of the final adult tube structure (Seydoux, Savage, & Greenwald, 1993) (see below). Following eversion, the vulva lumen remains in a closed conformation unless opened by contractions of the sex muscles, which attach to multiple vulva toroids (Sharma-Kishore et al., 1999). During L4 and adult stages, each vulva cell type expresses different combinations of known transcription factors, membrane fusogens, or other molecular markers (Inoue et al., 2004; Inoue et al., 2002; Inoue, Wang, Ririe, Fernandes, & Sternberg, 2005; Mok et al., 2015; Shemer et al., 2000;

Sternberg & Horvitz, 1989), but the biological distinctions among the seven cell types are not well understood.

A chondroitin proteoglycan (CPG)-rich luminal matrix is thought to form at the earliest stages of vulva tube morphogenesis, and to swell with water to exert a uniform pushing force for the lumen expansion (Gupta, Hanna-Rose, & Sternberg, 2012; Hwang, Olson, Brown, et al., 2003). Chondroitin antibodies stain the mid-L4 vulva lumen, though in a disorganized fashion that likely reflects matrix destruction by chemical fixatives (Bender, Kirienko, Olson, Esko, & Fay, 2007). Mutants defective in chondroitin biosynthesis have a narrow or “squashed” vulva lumen (Sqv phenotype) (Herman, Hartwig, & Horvitz, 1999; Hwang, Olson, Brown, et al., 2003). Genetic screens for Sqv mutants identified many components of the chondroitin biosynthesis pathway (Herman et al., 1999; Hwang, Olson, Brown, et al., 2003; Hwang, Olson, Esko, et al., 2003), but did not identify any specific chondroitin-modified proteins, suggesting redundant contributions of multiple CPGs. To date, mass spectrometry has identified 24 CPG carrier proteins in *C. elegans*, but it is not yet known which, if any, of these contribute to vulva lumen expansion (Noborn et al., 2018; Olson, Bishop, Yates, Oegema, & Esko, 2006). One of these known CPGs is FBN-1, a fibrillin-related ZP protein that is part of the worm’s transient embryonic sheath matrix that precedes the cuticle (Kelley et al., 2015; Labouesse, 2012; Noborn et al., 2018; Priess & Hirsh, 1986). Other pre-cuticle aECM proteins also have been observed within the vulva and other developing tubes (Forman-Rubinsky et al., 2017; Gill et al., 2016), and the adult vulva becomes cuticle-lined in adults (Page & Johnstone, 2007; Sulston & Horvitz, 1977). These observations suggested to us that a transient sheath-like aECM may exist within the developing vulva lumen.

aECM proteins show dynamic patterns of localization during vulva lumen morphogenesis

To examine aECM protein expression and localization in the vulva, we examined Superfolder (Sf) GFP or mCherry-based translational fusions generated by transgenic methods or (in most cases) by CRISPR-Cas9 genome editing of the endogenous loci (Materials and Methods). Six different aECM proteins were assessed (Figure 3A): the ZP proteins FBN-1 (Kelley et al., 2015), LET-653 (Gill et al., 2016) and NOAH-1 (Vuong-Brender et al., 2017), the lipocalin LPR-3 (Forman-Rubinsky et al., 2017), and the extracellular leucine-rich repeat only (eLRRon) proteins LET-4 (Mancuso et al., 2012) and SYM-1 (Davies, Spike, Shaw, & Herman, 1999; Vuong-Brender et al., 2017). We also examined a shortened version of LET-653 containing only the ZP domain, because prior studies had demonstrated that this domain is sufficient for matrix incorporation and excretory duct tube shaping (Gill et al., 2016) (Figure 3A). FBN-1, NOAH-1 and LET-4 each have transmembrane domains (but could be cleaved extracellularly), while LET-653, LPR-3 and SYM-1 are secreted proteins. These fusions permitted observations of matrix structure in live L4 animals, without the matrix destruction typically induced by chemical fixation for immunofluorescence. In each case, these fusion proteins were functional as assessed by mutant rescue or strain phenotypes (Materials and Methods), suggesting that their localization closely approximates the endogenous patterns. Each fusion protein initially appeared at around the L4.2 stage, and then exhibited a temporally and spatially distinct pattern over the course of L4 vulva morphogenesis (Figure 3B-D). All six matrix proteins were transient and disappeared in the adult stage, indicating that they are not components of the mature cuticle, but rather define a distinct matrix type present only during morphogenesis.

The ZP proteins FBN-1 and LET-653 showed somewhat complementary luminal patterns (Figure 3B,D). Beginning at L4.2, and as previously reported for LET-653(PAN domain) fragments (Gill et al., 2016), LET-653 decorated a core structure in the center of the lumen that rises to the level of the vulD and vulE cells, along with lateral elements that connect this core to the vulA, vulB1 and vulB2 cells and to the surrounding epidermis (Figure 3B,D). The central core structure could also be detected very weakly by DIC (Figure 2; red arrowhead). This core changed appearance during vulva eversion, but remained visible in the most ventral, 2°-cell-derived region through the L4.9 stage. Transiently, at the L4.3-L4.5 stages, LET-653 also weakly marked the apical membranes of most cells. Finally, FBN-1 overlapped with LET-653-marked structures near vulB1 and vulB2 surfaces, but otherwise was mainly excluded from the core area and instead filled the more dorsal part of the lumen above the core (Figure 3B,D). During vulva eversion, FBN-1 became excluded from the dorsal-most portions of the lumen lined by 1°-derived cells, such that LET-653 and FBN-1 together appeared to demarcate at least 3 separate luminal zones roughly corresponding to the regions outlined by the vulA/B cells, vulC/D cells, and vulE/F cells (Figure 3B).

The isolated LET-653 ZP domain and the other four aECM proteins marked specific apical membrane-proximal regions in a dynamic manner (Figure 3C,D). LET-653(ZP) specifically labelled just the 1°-derived vulE and vulF cell surfaces at L4.3-L4.5 stages. Previous Fluorescence Recovery After Photobleaching (FRAP) studies showed that, while it is present, this pool of LET-653(ZP) is relatively immobile, consistent with matrix incorporation (Gill et al., 2016). NOAH-1 faintly marked all 2° vulva cell surfaces at L4.4-L4.5, but then became increasingly concentrated on vulC and vulD. During vulva eversion, NOAH-1 prominently marked matrix spikes that protruded from vulC into the lumen, and these spikes attached to LET-653-marked lateral structures near vulB2 surfaces (Figure 3C,D). These NOAH-1—LET-

653 connections then persisted as the lumen narrowed. LPR-3 briefly marked all vulva cell apical surfaces at early L4.4, but then became restricted to 2° cells and then specifically to vulB1 and vulB2 before largely disappearing by L4.6-L4.7 (Figure 3D). The departure of LPR-3 from vulC and vulD coincided with the increasingly strong presence of NOAH-1 there. The transmembrane eLRRon protein LET-4 marked all vulval apical membranes during the late L4.2-L4.7 period, and thereafter appeared intracellular (Figure 3D). Finally, the secreted eLRRon protein SYM-1 showed the most limited pattern, labelling vulB1 and vulB2 for just a brief period at L4.4-L4.5 (Figure 3D). Together, these data reveal that different combinations of aECM factors assemble on the luminal surface of each vulva cell type. Furthermore, the precise timing of each factor's appearance and disappearance points to highly regulated mechanisms for matrix assembly and remodeling.

Ultrastructural features of the luminal matrix differ between 1° and 2°-derived vulva regions

Prior transmission electron microscopy (TEM) studies of the vulva (Gill et al., 2016; Herman et al., 1999) used chemical fixation methods that poorly preserved the luminal matrix and did not capture the complex luminal structures observed in the live imaging above. To obtain a clearer view of matrix ultrastructure, we turned to high pressure freezing (HPF) and freeze substitution (Hall, Hartwig, & Nguyen, 2012). This method achieved much better matrix preservation and revealed many matrix layers and fibrils that we could correlate with those observed by light microscopy. Serial thin sections were collected transverse or length-wise to the body axis to obtain a three-dimensional view. Images of mid-L4 (L4.4-L4.5) and late-L4 (L4.8-L4.9) stage vulvas are shown in Figures 4, 5 and S1, S2. A striking feature of both stages is the difference in matrix organization in the dorsal (1°-derived) vs. ventral (2°-derived) portions of the lumen.

235

236 At the mid-L4 stage, a rough granular matrix fills the entire vulva lumen, and embedded
237 within it are a central core structure and numerous ventro-lateral fibrillar elements similar to
238 those seen with LET-653::SfGFP (Figure 4B-E). Most of the dorsal lumen surrounding the
239 central core contains only the granular matrix; this corresponds to the region marked by FBN-
240 1::mCherry (Figure 3B) and likely contains additional CPGs. There is no single luminal channel
241 running through the granular matrix, which appears organized into multiple wide strips or flaps,
242 each edged with a more electron-dense border (Figure 4B,C). 1°-derived vulval cells have
243 relatively smooth apical surfaces lined with thin matrices that separate them from the granular
244 matrix (Figure 4F-H), while the 2°-derived cells have more protrusive apical surfaces lined with
245 numerous fibrils that are embedded within the granular matrix (Figure 4D-F,I,J).

246

247 At the dorsal apex of the vulva, the AC remnant hymen is lined by a layer of finer-
248 grained, electron-dense matrix that separates it from the vulva granular matrix (Figure 4K).
249 Within this AC matrix are numerous extracellular vesicles (EVs). The contents and purpose of
250 these EVs are not currently known, but the AC is a source of multiple signaling molecules (Hill &
251 Sternberg, 1992; Sherwood & Sternberg, 2003).

252

253 The vulF cells contain numerous large (~200 nm) secretory vesicles that resemble those
254 seen in mammalian goblet cells (Figure 4F,G; (Birchenough, Johansson, Gustafsson,
255 Bergström, & Hansson, 2015)). These vesicles contain globules that resemble mucin packets,
256 along with a few membranous intraluminal vesicles (ILVs). The secretory vesicles appear to be
257 dumping their contents within sequestered pockets at the left and right extremes of the lumen,
258 and these contents then expand spherically upon contacting the outside environment. The

contents within these luminal pockets are continuous with a thin membrane-proximal matrix layer that likely corresponds to the layer marked by LET-653(ZP)::SfGFP (see Figure 3D and below).

vulE surfaces are decorated by a mesh-like matrix that drapes down along the top border of the core and ventro-lateral fibrils (Figure 4H). This matrix appears as dark membrane-associated patches when vulE is viewed in cross-section (Figure 4F,G). This matrix may serve as the barrier that excludes FBN-1 from the ventral fibrillar region (see Figure 3B,D).

vulD and vulC surfaces that sit above the ventro-lateral fibrils (and external to the core) are lined with thin fibrils that run in a dorsal-ventral orientation, parallel to the cell membranes (Figure 4I). These fibrils are embedded within the granular luminal matrix rather than forming a separate layer, and they abut numerous small cellular projections. The fibrils are particularly concentrated in narrow (~0.5 micron) lumen pockets generated by the complex shape of vulD (Figure 4F). These fibrillar regions correspond to those surfaces that become strongly marked by NOAH-1::mCherry (see Figure 3C).

Finally, the ventral-most vulC surfaces, as well as vulB2, vulB1 and vulA, interface with the dense ventro-lateral fibrils, which run both perpendicular to and parallel with the cell membranes (Figure 4B,E). The cell surfaces that interface with these fibrils are extremely protrusive (Figure 4J). At the most ventral edge of the lumen, beneath the core fibrils, matrix layers that resemble those of the epidermal sheath and nascent cuticle interface with the remaining L4 epidermal cuticle (which has broken and pulled away somewhat in this specimen) (Figure 4B,E,J).

The late-L4 stage vulva (Figure 5) retains several of the matrix features seen at the earlier stage, with some notable differences. An electron dense “plug” resembling the earlier AC matrix is present at the dorsal apex and contains EVs (Figure 5A,B,F). A similar-appearing matrix is also present at the ventral opening of the lumen (Figure 5A,D). The 1°-derived vulE and vulF cells and the 2°-derived vulC and vulD cells are now covered with a thick membrane-proximal matrix that somewhat resembles the prior CPG matrix, but with a well-defined, darkly staining border and a single open channel that runs through its center (Figure 5A,B,F). The membrane-proximal matrix over vulC and vulD also contains many dense fibrils that extend down into the matrix below (Figure 5C,D); these likely correspond to the NOAH-1-marked matrix spikes observed by confocal imaging (see Figure 3C). The remaining vulA, vulB1 and vulB2 cells are covered with a more complex, multi-layered matrix that resembles the nascent pre-cuticle on nearby epidermal cells (Figure 5D,E). Various fibrillar structures are embedded within this thick matrix (Figure 5D), possibly corresponding to the core and ventrolateral fibrils seen earlier. Thus, just as seen by confocal light microscopy at this stage (Figure 3B), TEM shows 3 distinct luminal zones corresponding to the regions outlined by the vulA/B cells, vulC/D cells, and vulE/F cells.

1° and 2° vulva cell types produce and assemble different matrices

To better understand the differences between the matrix produced and assembled by 1° vs. 2° vulva cell types, we analyzed matrix patterns in *lin-12*/Notch mutants. LIN-12/Notch promotes 2° vs. 1° VPC fates, so loss-of-function [*lin-12(0)*] mutants have only 1° vulva cell types, while gain-of-function [*lin-12(d)*] mutants have only 2° vulva cell types (Greenwald, Sternberg, & Horvitz, 1983; Sternberg & Horvitz, 1989). *lin-12(0)* and *lin-12(d)* mutants both have well-inflated (though mis-shapen) vulva lumens (Figure 6), indicating that relevant CPGs are made by both sets of vulva cell types. Indeed, Herman et al (Herman et al., 1999) previously

showed that both types of *lin-12* mutants require the *Sqv* chondroitin biosynthesis pathway for lumen inflation.

Close examination of *lin-12* mutants suggested, however, that the central core structure was missing. When LET-653::SfGFP was introduced into *lin-12(0)* mutants, core structures appeared very meager or absent (Figure 6B). In *lin-12(d)* mutants, no core was observed in the central lumen, but some ventro-lateral elements were still present at the vulB “fingers” (Figure 6C). We conclude that both 1° and 2° cells are required to generate the core, but that 2°-derived cells (most likely vulB1 and vulB2) generate at least some of the ventrolateral elements independently.

lin-12 mutants also showed changes in the localization of membrane-proximal matrix factors, as predicted based on the cell fate changes. For example, LET-653(ZP) marked all vulva apical membranes in *lin-12(0)* mutants, but none in *lin-12(d)* mutants (Figure 6). Since *let-653* is expressed by all seven vulva cell types (Gill et al., 2016), these data suggest that a 1°-specific partner is required to recruit LET-653(ZP) to the membrane-proximal matrix. In contrast, NOAH-1 was mostly absent from vulva apical membranes in *lin-12(0)* mutants, but strongly marked the dorsal-most apical membranes in *lin-12(d)* mutants (Figure 6). LPR-3 marked some apical membranes in both *lin-12(0)* and *lin-12(d)* mutants, but was more robust in the latter, consistent with its 1° and 2° membrane-binding patterns in wild type (Figure 6). In summary, the results of these experiments indicate that each cell’s identity, rather than its position in the organ, determines what matrix factors assemble on its surface.

MUP-4/matrillin expression coincides with appearance of mature cuticle

The continuous movement of cells and the changes in aECM composition during vulva morphogenesis, including the eventual transition from pre-cuticle aECM to cuticle, suggest

dynamic cell-cell and cell-aECM attachments. If or how the above aECM proteins attach to apical membranes remain unknown, particularly since most either do not have transmembrane domains (Figure 3A), do not require their transmembrane domains for function (Mancuso et al., 2012), or are likely cleaved to release the extracellular domains from their transmembrane domains (Bokhove & Jovine, 2018). Body cuticle attaches to cell surfaces via hemidesmosome-like structures (CeHDs) and fibrous organelles (FOs) that span the epidermis and link to body muscle (Pásti & Labouesse, 2014). Apically, the CeHD component VAB-10a (related to spectraplakins) (Bosher et al., 2003) links to the matrilin-like transmembrane proteins MUP-4 (Hong et al., 2001) and MUA-3 (Bercher et al., 2001) to connect the epidermis and cuticle (Suman et al., 2019). However, it is not known whether similar complexes also link other types of aECMs to epithelial cells, particularly in regions where body muscle is not adjacent.

To address whether the known matrix-anchoring complexes could anchor aECMs in the vulva, we asked where VAB-10a and MUP-4 appear in vulval cells. VAB-10::GFP was present along apical membranes of all vulva cells throughout L4 morphogenesis (Figure 7A). However, MUP-4::GFP appeared only later, at the L4.6-L4.7 stage, and was enriched over vulC and vulD, where the vm1 sex muscles attach (Figure 7B). By L4.9 and adult, when cuticle is present, MUP-4::GFP lined all vulva apical membranes, but it was expressed most prominently in the vulA toroid, which links the vulva to the surrounding epidermis and body muscle (Figure 7B). Therefore, while MUP-4 and VAB-10 could potentially help connect the cuticle to vulva cells just as they do in the epidermis, different (possibly also VAB-10-affiliated) linkers likely recruit the earlier pre-cuticle aECM factors. Consistent with this hypothesis, prior large-scale RNAi studies revealed protruding vulva defects (indicative of abnormal eversion) after depletion of vab-10, but not after depletion of mup-4 or mua-3 (Shephard, Adenle, Jacobson, & Szewczyk, 2011; Simmer et al., 2003). Further experiments will be needed to test the roles of VAB-10, MUP-4

and MUA-3 more definitively, and to identify the mechanisms that link aECM to vulva apical membranes.

Transient aECM factors facilitate proper vulva eversion

The complex localization patterns described above suggest important roles for aECM factors in vulva morphogenesis. Of the six aECM factors described here, only *sym-1* mutants are fully viable, while presumed null mutants of the rest mostly arrest as L1 larvae with excretory tube blockage or other epithelial tissue-shaping defects (Forman-Rubinsky et al., 2017; Gill et al., 2016; Mancuso et al., 2012; Pu, Stone, Burdick, Murray, & Sundaram, 2017; Soulavie, Hall, & Sundaram, 2018; Vuong-Brender et al., 2017). To examine vulva phenotypes in these lethal mutants, we took advantage of rare escapers (for *fbn-1*) or used tissue-specific rescue strains (Materials and Methods) to bypass the earlier requirements (for *let-653* and *let-4*). We were not able to examine *noah-1* or *lpr-3* mutants in this study because of their severe epidermal molting defects (Forman-Rubinsky et al., 2017; Vuong-Brender et al., 2017). All mutants examined had fairly normal vulva lumens at the mid-L4 stage, indicating efficient CPG-dependent lumen inflation (Gill et al., 2016) (Figure 8A). All mutants also assembled a core structure, as seen by DIC (Figure 8A). However, in some cases, later stage vulvas appeared misshapen or improperly everted (Figure 8A). Specifically, some *let-653* mutants had a prematurely collapsed vulva lumen (Figure 8A, asterisk), and most *fbn-1* mutants had abnormal bulges of the outer vulA, vulB1 and vulB2 cells (Figure 8A, arrowheads). We conclude that aECM factors facilitate later stages of vulva morphogenesis, including vulva eversion.

To better understand these phenotypes, we focused on *let-653* mutants. As adults, most *let-653* mutants were able to lay eggs; however, a small proportion of mutants ruptured at the vulva and/or were Egg-laying defective (Egl) (Figure 8B). Measurements of the 1°- and 2°-derived portions of the vulva lumen confirmed normal dimensions at the L4.4 stage, but slightly reduced

dimensions in a subset of animals at the onset of eversion at the L4.7 stage (Figure 8C, Figure 8-1). A transgene expressing just the LET-653(ZP) domain reversed the L4.7 defects, and led to overexpansion of the lumen at L4.4 (Figure 8C, Figure 8-1), consistent with our prior report (Gill et al., 2016) that this domain has lumen-expanding properties.

Vulva eversion has been described as the vulva “turning inside out” (Seydoux et al., 1993; Sharma-Kishore et al., 1999), but the specific cellular events involved have never been reported. To visualize cell positions and shapes during eversion, we used the RhoG marker MIG-2::GFP to label all vulva cell membranes (Figures 2, 8D,E), and the *daf-6pro::CFP* and *egl-17pro::YFP* marker combination (Mok et al., 2015) to label the vulE/F and vulC/D cells specifically (Figure 8F). During wild-type eversion (Figure 8D), all four of these cells elongate in the dorsal-ventral axis to partly occlude the luminal space. vulC extends a narrow NOAH-1 matrix spike into the core matrix, whose spokes appear to fold like those of an umbrella as the lumen narrows (Figure 3C). The vm1 sex muscles also extend ventrally into vulC and vulD (Figures 2, 8D). Meanwhile, vulA, vulB1 and vulB2 tilt ventrally, while vulE reaches dorsally to connect to the seam epidermis. By adulthood, vulE and vulF enclose the bulk of the lumen, vulC and vulD form the vulva lips, and the vulA, vulB1 and vulB2 cells are excluded from the lumen, and instead form the epidermis surrounding the vulva opening (Figures 2, 8D,F).

In *let-653* mutants, vulva eversion occurred in a more irregular manner (Figure 8). The anterior and posterior halves of the vulva showed various asymmetries by the onset of eversion at the L4.7 stage (Figure 8E), and cell shapes and relative cell positions continued to be variably abnormal in older L4s and adults (Figure 8F). Defects were particularly noticeable in parasagittal slices and in 3D reconstructions of the YZ dimensions; whereas WT adult vulE cells reach far dorsally to connect to the lateral seam epidermis on the left and right sides of the body (Sharma-Kishore et al., 1999), some *let-653* vulE cells appeared not to reach that far (Figure

8F). Imaging of a cell junction marker revealed that let-653 morphogenesis defects are not due to failure of cell fusion to form the vulva toroids (Figure 8-2). Instead, we conclude that LET-653 plays subtle roles to coordinate the complex cell shape changes that occur during the process of eversion.

LET-653 is required for multiple aspects of vulva aECM organization

To test how LET-653 affects the organization of the vulva matrix, we first assessed the status of other matrix factors in the let-653 mutant background. let-653 mutants still assembled some type of central core structure, as seen by DIC (Figure 8A) and by the exclusion of FBN-1 from this region (Figure 9A). As in WT, FBN-1 departed from the dorsal-most lumen during eversion (Figure 9A) and LPR-3 and NOAH-1 still appeared at their proper locations (Figure 9B). However, the normally precise sequence of LPR-3 clearance was disrupted, such that LPR-3 remained on vulC and vulD apical surfaces longer than normal, and overlapped significantly with NOAH-1 there (Figure 9B), suggesting improper organization of the vulC/D membrane-proximal aECM.

TEM of a mid-L4 let-653 mutant revealed more dramatic matrix abnormalities (Figure 9C-C'). Some vulF secretory vesicles contained very disorganized, dark aggregates, and the membrane-proximal matrices over vulF, vulE, and the AC/utse appeared filled with such aggregates (Figure 9C'). The luminal matrix also contained many aggregates or short, fibrillar structures rather than having the uniform granular appearance of WT. Few fibrils were detected near the surfaces of vulC/D or other 2°-derived cell types. Instead, many long fibrils accumulated at the dorsal apex of the vulva, along the AC/utse, where fibrils had not been seen in WT (Figure 9D, Figure 4-1). The central core region was recognizable but less well-defined than in WT, as it was interspersed with many aggregates or short fibrils similar to those present in the rest of the luminal matrix (Figure 9C, Figure 4-1). Thus, although let-653 is not required to

build the luminal core or to establish membrane-proximal matrices per se, it is required for the proper morphology of these structures and to set up the major dorsal vs. ventral differences in the granular vs. fibrillar organization of the vulva aECM.

Vulva aECM structures form independently of chondroitin

Thus far, the data indicate that chondroitin plays an early role in vulva lumen inflation, whereas LET-653 and FBN-1 play later roles in morphogenesis and eversion. However, FBN-1 is a known CPG (Noborn et al., 2018) and other aECM factors appear to be embedded within the CPG matrix (Figure 4), suggesting some coordination between the two processes.

To ask if chondroitin affects aECM assembly, we examined aECM reporters in *sqv-5* and *mig-22* mutants (Figure 10). *sqv-5* and *mig-22* encode chondroitin sulfate synthases related to human CHSY1 and CHSY2 (Hwang, Olson, Brown, et al., 2003; Suzuki, Toyoda, Sano, & Nishiwaki, 2006), which promote chondroitin biosynthesis and polymerization (Izumikawa et al., 2004). LET-653(ZP) did still assemble on the apical surfaces of 1° cells in *sqv-5* mutants (Figure 10A). However, these null mutants have a very narrow vulva lumen, which made it difficult to stage L4 animals accurately and assess the localization of full length LET-653 or other dynamic aECM factors. Therefore, we turned to *mig-22* hypomorphic (*rf*=reduced function) mutants, which have a slightly less severe vulva phenotype.

In *mig-22(rf)* mutants at mid-L4 stage, both the 1°- and 2°-derived parts of the lumen were narrower than in wild-type, but lumen length varied between regions (Figures 10B,C and 11A,B). The vulva "neck" region, defined by *vulD*, *vulE* and *vulF* (see Figure 2), was longer than in wild type, and *vulD* cells were prematurely elongated along the dorsal-ventral axis (Figure 10B), as previously described for *sqv-3* mutants (Herman et al., 1999). In contrast, the main

body of the lumen, defined by vulA, vulB1, vulB2, and vulC, was shorter. Thus chondroitin has very different effects on the apical domain size of different cell types.

mig-22(rf) mutants still had a luminal core structure marked by LET-653::SfGFP, though this was narrower than in wild-type, matching the changed dimensions of the lumen (Figure 10D). mig-22(rf) mutants also still recruited LET-653(ZP), NOAH-1 and LPR-3 to appropriate apical surfaces (Figure 10A,E). Thus, chondroitin does not appear essential for assembling the vulva aECM, though it remains possible that it influences aECM structure in a more subtle way.

Chondroitin and the vulva aECM have both lumen expanding and lumen constraining properties

To ask if chondroitin and aECM factors work cooperatively to shape the vulva, we examined double mutants between mig-22(rf) and let-653. Surprisingly, loss of let-653 largely suppressed the mig-22(rf) mutant Sqv phenotype. At the L4.4 stage, double mutants appeared properly inflated in the ventral region, and actually overly inflated in the dorsal, 1°-derived region (Figure 11A,B). Nevertheless, at later eversion stages, the vulva lumen appeared variably abnormal and contained disorganized matrix material (Figure 11C), and as adults, almost all double mutants were Egl or ruptured at the vulva (Figure 11D). These results indicate that MIG-22 and LET-653 have opposing roles in promoting vs. restraining initial lumen inflation, but also have cooperative roles in restraining the subsequent expansion of the dorsal-most 1° vulva toroids, and in promoting later steps of eversion and cuticle formation. These results are inconsistent with the model that chondroitin acts only to exert a uniform hydrostatic expansion force. Rather, as shown here, chondroitin proteoglycans act within a complex luminal scaffold that likely exerts, resists, and distributes multiple different types of vulva cell- and lumen-shaping forces.

Discussion

The diameter of a tube lumen is ultimately determined by the shape and organization of the cells that surround that lumen. Two well-known determinants of cell shape are the cytoskeleton and the ECM. Here, we showed that the luminal aECM within the developing *C. elegans* vulva tube has a structural and functional complexity that rivals that of the cytoskeleton. The cytoskeleton consists of multiple dynamic and interacting components (actin, microtubules, and intermediate filaments) that are organized into both cytosolic and membrane-anchored fibrils and webs (Fletcher & Mullins, 2010). These cytoskeletal elements can exert both pushing and pulling forces on cell membranes (Fletcher & Mullins, 2010). Similarly, the vulva luminal matrix contains a variety of both free and seemingly membrane-attached structural elements. These elements are cell-type specific and highly dynamic over the course of tube morphogenesis. Removal of individual aECM elements, or sets of elements, has distinct effects on cell and lumen shape, revealing both lumen expanding and lumen constricting roles. Ultimately, these data reveal a complex and dynamic aECM which offers a powerful model for investigating aECM assembly, remodeling, and tube-shaping capacity.

Multiple types of matrix shape the vulva lumen

Although it has been clear for over a decade that chondroitin GAGs are required to inflate the vulva lumen (Herman et al., 1999; Hwang & Horvitz, 2002a, 2002b; Hwang, Olson, Brown, et al., 2003; Hwang, Olson, Esko, et al., 2003), other aECM factors involved in shaping had not been previously described. Here, we showed that the vulva aECM contains multiple discrete elements (Figure 12). First, a granular matrix containing the CPG FBN-1 (and likely many others) fills the luminal cavity by mid-L4. Second, distinct types of membrane-proximal aECMs line different vulva cell types at different stages; these aECM layers contain ZP domain, eLRRon and lipocalin proteins and appear to be analogous to the embryonic sheath that lines the epidermis (Mancuso et al., 2012; Priess & Hirsh, 1986; Vuong-Brender et al., 2017). Third, a

stalk-like core structure forms within the central lumen; this core is marked by the ZP protein LET-653 via its PAN domains (Gill et al., 2016). Finally, the core attaches to different aECM-covered cell surfaces via ventrolateral fibrils, also marked by LET-653 PAN domains. Each of these elements may play different roles in lumen shaping (Figure 12).

The six matrix proteins analyzed here are probably a very small subset of the total components that make up the various vulva aECM structures, and for the most part their roles in building these structures remain to be tested. We showed that *let-653* is broadly important for proper morphology of the membrane-proximal matrices over the AC/utse, *vulE/F*, and *vulC/D*, and for restricting fibrillar structures to their proper ventral locations. Neither LET-653 nor any of the other aECM proteins tested is required to build the luminal core structure, but loss of this structure in *lin-12*/Notch mutants suggests that both 1°- and 2°-derived factors are involved.

Apical matrix may generate, counteract and distribute multiple forces during lumen shaping

Prior work showed that the vulva is expanded by a combination of pushing forces by chondroitin GAGs (Hwang, Olson, Brown, et al., 2003) and actin-myosin constriction by 2° cells, which may then focus the GAG-dependent forces dorsally (Yang, Roiz, Mereu, Daube, & Hajnal, 2017). The data here suggest that GAGs not only inflate the lumen, but also play other roles. First, chondroitin depletion does not affect all vulva cells in the same way; in *mig-22(rf)* mutants, some cells have expanded apical domains, while others have shortened apical domains. Second, in the context of *let-653* loss, *mig-22(rf)* actually causes increased dorsal lumen expansion, revealing a lumen-constraining role for both LET-653 and chondroitin (Figure 11). Finally, the predominant defect in *fbn-1* single mutants is not in lumen inflation, but instead in vulva eversion, showing that GAG-modified proteins have diverse functions in vulva shaping.

The other aECM factors described here may counteract and distribute the forces exerted by GAGs and the cytoskeleton, or may themselves generate additional types of forces. The

vulE/F aECM and central core component LET-653 restrains CPG-dependent lumen inflation in early-to-mid-L4 stages, but also helps maintain lumen inflation during the subsequent steps of vulva morphogenesis. Interestingly, LET-653 impacts these later steps even though the functional LET-653(ZP) domain is no longer visible at those stages. LET-653(ZP) and other aECM components may form a membrane-anchored scaffold whose assembly at mid-L4 initially “locks in” a particular lumen size to prevent further CPG-dependent inflation (Figure 12). This transient scaffold could then serve as a template for recruitment and assembly of later matrix factors, including cuticle collagens, that will sculpt the final structure. Through unknown mechanical connections with membranes and the cytoskeleton, aECM factors also may influence the cytoskeletal organization of vulva cells to promote their rearrangements and cell shape changes. Connections among aECM, vulva cells, and sex muscles could serve as anchor points to transmit muscle-generated forces, as proposed for epidermal elongation in the embryo (Vuong-Brender et al., 2017). Finally, the LET-653-marked core structure and associated fibrils appear to constrict during lumen narrowing, and such matrix re-organization could potentially exert a pulling force on apical membranes (Figure 12), as has been proposed for alae (cuticle ridge) formation (Sapio, Hilliard, Cermola, Favre, & Bazzicalupo, 2005).

Multiple aECM factors likely cooperate in vulva lumen shaping with LET-653. Most aECM single mutants, including *let-653*, have only subtle vulva shaping defects and a low percentage of egg-laying defective adults, despite drastic defects in matrix organization (Figures 8, 9). This is in contrast to the much more penetrant and dramatic phenotypes observed in these same mutants in shaping narrow excretory system tubes (Gill et al., 2016; Mancuso et al., 2012) or the embryonic epidermis (Vuong-Brender et al., 2017). The vulva appears to be less sensitive to defects in aECM than these other tissues, possibly because its large lumen can tolerate many irregularities in cell shape and still remain passable for egg-laying.

LET-653 and cell type-specific partners may traffic through large secretory vesicles in vulF

Individual aECM components appear and disappear from individual cell surfaces at specific timepoints. These localization patterns suggest careful regulation. How are these proteins, and their corresponding aECM layers, built and broken down at the correct times and places? Part of the answer may lie in time- and cell-type-specific secretion.

Many secreted matrix proteins are packaged and trafficked via specialized vesicles. For example, collagens are secreted from extra-large vesicles (Malhotra & Erlmann, 2015) and then processed after secretion to enable their assembly (Holmes, Lu, Starborg, & Kadler, 2018). Different ZP proteins secreted from the same cell are sorted into separate pools of vesicles, possibly to prevent their premature association (Jovine, Qi, Williams, Litscher, & Wassarman, 2007). In fact, we observed large vesicles emptying material into the vulva lumen from vulF (Figure 4). LET-653 is a potential cargo within these secretory vesicles and may traffic with one or more partners that form the membrane-proximal aECM over vulE/F. In the absence of LET-653, vesicle contents appear to aggregate abnormally as soon as they are exposed to the luminal environment. Although LET-653 is expressed by all vulva cell types, it may traffic in different types of vesicles or with different partners in each cell type, explaining why LET-653(ZP) does not form the same type of matrix over all vulva cells, and why abnormal vesicles were not observed in other vulva cells in let-653 mutants.

The vulF secretory vesicles resemble mucin vesicles found in goblet cells of the mammalian lung and gut. Tightly compressed mucin packets in those vesicles are thought to expand rapidly upon reaching the luminal environment due to changes in pH and salt conditions (Birchenough et al., 2015); the CFTR ion channel, which is mutated in cystic fibrosis patients, is expressed on adjacent cell types (Kreda, Davis, & Rose, 2012) and is important for establishing the proper luminal environment for mucin expansion to occur (Kreda et al., 2012). Given that

591 vulF secretory vesicles empty into narrow lumen compartments between vulF and vulE, it is
592 possible that vulE expresses key ion channels or other matrix factors that are important for
593 proper assembly of the extruded matrix.

594

595 The vulva as a system for visualizing and dissecting aECM trafficking and assembly

596 Classic TEM studies in many systems have shown that aECMs are layered structures
597 (Chappell et al., 2009; Johansson et al., 2011). However, a major challenge for understanding
598 aECMs has been the difficulty in visualizing them in a more high-throughput manner. The large
599 size of the vulva lumen, combined with the transparency of *C. elegans*, allowed us to visualize
600 the various aECM elements by light microscopy in a way that is unprecedented in other
601 systems. The vulva therefore provides a very powerful system for addressing further
602 mechanistic questions regarding how aECM components traffic to the apical surface, how
603 aECM structures are assembled and remodeled, and how they ultimately impact cell and tube
604 shape.

Materials and Methods

Worm strains, alleles and transgenes

See Table 1 and Key Resources Table for a complete list of all strains, alleles and transgenes used. All strains were derived from Bristol N2 and were grown at 20°C under standard conditions (Brenner, 1974). *let-653* and *let-4* mutants were obtained from mothers rescued with wild-type transgenes expressed in the excretory system under the control of the *lin-48* or *grl-2* promoters (Forman-Rubinsky et al., 2017). Prior tissue-specific rescue experiments showed that LET-653 (Gill et al., 2016) and LET-4 (Mancuso et al., 2012) have little or no ability to travel between tissues. Consistent with this, *lin-48pro::LET-653::SfGFP* did not drive any detectable GFP expression in the vulva. *sqv-5* mutants were obtained from heterozygous mothers. All other mutants were obtained from homozygous mothers.

Transgene *aaals12* [*fbn-1pro::FBN-1::mCherry*; *ttx-3pro::GFP*] was derived from array *aaaEx78* (Katz et al., 2018) and expresses full-length FBN-1 tagged internally with mCherry inserted just prior to the ZP domain. *aaaEx78* rescued *fbn-1(tm290)* molt defects and other lethality from 85% (n=236) in non-transgenic siblings to 10% (n=1676) in transgenic animals.

CRISPR/Cas9-mediated generation of reporters

To generate LET-653::SfGFP and SfGFP::LPR-3 fusions via CRISPR, a self-excising cassette (SEC) vector containing SfGFP was generated (pJC39). SfGFP was amplified and inserted a larger fragment of the SEC vector pDD282 (Dickinson, Ward, Reiner, & Goldstein, 2013) via PCR sewing. The large fragment was inserted into pDD282 as a *NaeI* – *BglII* fragment. Henceforth, CRISPR was carried out as described (Dickinson, Pani, Heppert, Higgins, & Goldstein, 2015). Briefly, LET-653 or LPR-3 homology arms were inserted into the resulting plasmid and the relevant PAM sites were then mutated via site-directed mutagenesis. sgRNAs

were generated via site-directed mutagenesis that inserted a primer encoding the gRNA before a U6 promoter in the plasmid pDD162 (Dickinson et al., 2013). These plasmids were injected into N2 hermaphrodites. F2 progeny were screened by microscopy for Hygromycin resistance and/or SfGFP fluorescence. Insertions were verified by PCR and Sanger sequencing. SfGFP was inserted immediately before the LET-653 stop codon or immediately following the LPR-3 signal peptide. An SEC inserted into an intron within the SfGFP coding sequence was removed via heat shock (Dickinson et al., 2015). Excision was confirmed by PCR and Sanger sequencing.

The mCherry::LET-4 fusion was generated using the SapTrap method (Schwartz & Jorgensen, 2016). LET-4 homology arms were inserted into plasmid pMLS291 using SapI digestion and ligation. The resulting plasmid was co-injected into N2 hermaphrodites with a plasmid containing relevant sgRNAs inserted into pDD162 (Dickinson et al., 2013). F2 progeny were screened by microscopy for mCherry fluorescence. Insertions were verified by PCR and Sanger sequencing. mCherry was inserted immediately after the LET-4 signal sequence.

All CRISPR fusion strains were evaluated for viability. *let-653(cs262[LET-653::SfGFP])* was 93% viable (n=195), *lpr-3(cs250[SfGFP::LPR-3])* was 98% viable (n=137), and *let-4(cs265[mCherry::LET-4])* was 100% viable (n=154).

Staging and microscopy

Larvae were staged by vulva morphology. Fluorescent, Brightfield, Differential interference contrast (DIC), and Dodt (an imaging technique that simulates DIC) (Dodt & Zieglgansberger, 1990) images were captured on a compound Zeiss Axioskop fitted with a Leica DFC360 FX camera or with a Leica TCS SP8 confocal microscope (Leica, Wetzlar Germany). Images were processed and merged using ImageJ.

656
657 For TEM, L4 hermaphrodites from N2 (wild-type) or UP3342 (let-653(cs178);
658 csEx766[lin-48pro::LET-653::SfGFP; myo-2pro::GFP]) strains were fixed by high pressure
659 freezing followed by freeze substitution into osmium tetroxide in acetone (Weimer, 2006), and
660 then rinsed and embedded into LX112 resin and cut into serial thin sections of approximately 70
661 nm each. Sections were observed on a JEM-1010 transmission electron microscope (Jeol,
662 Peabody Massachusetts). Images were processed in ImageJ and manually pseudo-colored in
663 Adobe Illustrator (Adobe, San Jose California). We imaged vulvas for n=1 mid-L4 N2, n=2 late
664 L4 N2, and n=1 mid-L4 UP3342. Data for all animals are shown.

665

666 Lumen measurements

667 Vulva dimensions were measured using the box tool in ImageJ. Boxes were drawn
668 within the lumen in DIC images and their length and width were recorded. A minimum of 10
669 animals were examined for each experiment. vulD aspect ratio was measured by tracing the cell
670 outline from a single sagittal confocal Z-slice and then using the shape measurement tool in
671 ImageJ. The two vulD cells from each animal were treated separately. All measurements were
672 performed by a researcher blinded to genotype. Statistics were calculated using Prism software
673 (Graphpad, San Diego California) using two-tailed Mann-Whitney U tests.

674

675 Data availability statement

676 Strains used are listed in Table 1. All strains are available upon request.

677

Acknowledgements

We thank Ken Nguyen (Albert Einstein School of Medicine) and Biao Zuo and Inna Martynyuk (UPenn Electron Microscopy Resource Lab) for assistance with TEM, Andrea Stout (UPenn CDB Microscopy Core) for training and assistance with confocal imaging, Lily Zekavat for assistance with *lin-12* experiments, Michel Labouesse for strains, and John Murray, Nick Serra, Susanna Birnbaum, Hasreet Gill, Dave Matus, and members of the Matus laboratory for helpful discussions and comments on the manuscript. Some strains were provided by the CGC, which is funded by the NIH Office of Research Infrastructure Programs (P40 OD010440). This work was funded by NIH grants R01GM58540, R01GM125959, and R35GM136315 to M.V.S., T32 GM008216 and T32 AR007465 to J.D.C., and NIH OD010943 to D.H.H, and by ACS grant RSG-12-149-01-DDC to A.R.F.

691 **Table 1. Strains used in this work**

Strain	Genotype
ARF335	fbn-1(tm290) III; aaaEx78 [fbn-1pro::FBN-1::mCherry; ttx-3pro::GFP] (Katz et al., 2018)
ARF379	aaals12 [fbn-1pro::FBN-1::mCherry; ttx-3pro::GFP] V (Katz et al., 2018)
ARF359	upls1 [MUP-4::GFP; rol-6(su1006)] V; aaaEx78 [fbn-1pro::FBN-1::mCherry; ttx-3pro::GFP] (Hong et al., 2001; Katz et al., 2018)
HM24	upls1 V; aaals12 V (Hong et al., 2001; Katz et al., 2018)
GOU2043	vab-10(cas602 [vab-10a::gfp]) I (Y. Yang et al., 2017)
JU486	mfls4 [egl-17pro::YFP; daf-6pro::CFP; unc-119(+)] (Mok et al., 2015)
ML2482	noah-1(mc68 [NOAH-1::mCH(int)]) I (Vuong-Brender et al., 2017)
ML2547	sym-1(mc85 [SYM-1::GFP]) X (Vuong-Brender et al., 2017)
ML2615	dlg-1(mc103 [DLG-1::GFP]) X (Vuong-Brender et al., 2017)
N2	WT
NF68	mig-22(k141) III (Suzuki et al., 2006)
SP2163	sym-1(mn601) X (Niwa et al., 2009)
UP2386	csEx358 [lpr-1pro::LET-653b; unc-119pro::GFP] (Gill et al., 2016)
UP3244	let-653(cs178) IV; csEx358 (Gill et al., 2016)
UP3342	let-653(cs178) IV; csEx766 [lin-48pro::LET-653b::SfGFP; myo-2pro::GFP] (Forman-Rubinsky et al., 2017)
UP3349	aaals12 V; csIs64 [let-653pro::LET-653b::SfGFP; rol-6(su1006)]
UP3353	let-653(cs178) IV; aaals12 V; csEx766
UP3422	csIs66 [let-653pro::LET-653(ZP)::SfGFP; let-653pro::PH::mCherry] X
UP3444	sqv-5(n3611)/hT2 [bli-4(e937) let-?(q782) qIs48] I,III; csIs66 X
UP3462	let-653(cs178) IV; csIs66 X
UP3666	lpr-3(cs250 [ssSfGFP::LPR-3]) X
UP3693	noah-1(mc68 [NOAH-1::mCH(int)]) I; lpr-3(cs250 [ssSfGFP::LPR-3]) X
UP3746	let-653(cs262 [LET-653::SfGFP]) IV
UP3756	let-4(cs265 [ssmCherry::LET-4]) X
UP3757	dpy-19(e1259) lin-12(n137)/ hT2 [bli-4(e937) let-?(q782) qIs48] I,III; csIs66 X
UP3758	unc-32(e189) lin-12(n137 n720)/hT2 [bli-4(e937) let-?(q782) qIs48] I,III; csIs66 X
UP3788	noah-1(mc68 [NOAH-1::mCH(int)]) I; let-653(cs262 [LET-653::SfGFP]) IV
UP3856	let-653(cs262 [LET-653::SfGFP]) IV; let-4(cs265 [ssmCherry::LET-4]) X
UP3861	mulS27 [MIG-2::GFP; dpy-20+]; let-4(cs265 [ssmCherry::LET-4]) X (Honigberg & Kenyon, 2000)
UP3939	let-4(mn105) X; csEx819 [grl-2pro::LET-4; myo-2pro::mRFP] (Forman-Rubinsky et al., 2017)
UP3967	mig-22(k141) III; let-653(cs178) IV; csEx766
UP3968	mig-22(k141) III; let-653(cs178) IV; csEx766
UP3970	mig-22(k141) III; csIs66 X
UP3979	let-653(cs178) IV; dlg-1(mc103 [DLG-1::GFP]) X; csEx766
UP3995	mulS28 [MIG-2::GFP; unc-31+] (Honigberg & Kenyon, 2000)

UP3966	noah-1(mc68 [NOAH-1::mCH(int)]) I; let-653(cs178) IV; lpr-3(cs250 [ssSfGFP::LPR-3]) X; csEx766
UP4004	mig-22(k141) III; muls28
UP4005	let-653(cs178) IV; muls28; csEx766
UP4014	noah-1(mc68 [NOAH-1::mCH(int)]) I; mig-22(k141) III; lpr-3(cs250 [ssSfGFP::LPR-3]) X
UP4025	noah-1(mc68 [NOAH-1::mCH(int)]/hT2 [bli-4(e937) let-?(q782) qls48] I; unc-32(e189) lin-12(n137 n720)/hT2 [bli-4(e937) let-?(q782) qls48] III
UP4027	mig-22(k141) III; let-653(cs262 [LET-653::SfGFP]) IV
UP4038	unc-32(e189) lin-12(n137 n720)/hT2 [bli-4(e937) let-?(q782) qls48] I,III; lpr-3(cs250 [ssSfGFP::LPR-3]) X
UP4039	mig-22(k141) III; mfls4
UP4040	let-653(cs178) IV; mfls4; csEx766
UP4042	unc-32(e189) lin-12(n137 n720)/hT2 [bli-4(e937) let-?(q782) qls48] I,III; let-653(cs262 [LET-653::SfGFP]) IV
UP4043	dpy-19(e1259) lin-12(n137)/ hT2 [bli-4(e937) let-?(q782) qls48] I,III; lpr-3(cs250 [ssSfGFP::LPR-3]) X
UP4044	dpy-19(e1259) lin-12(n137)/ hT2 [bli-4(e937) let-?(q782) qls48] I,III; let-653(cs262 [LET-653::SfGFP]) IV
UP4045	noah-1(mc68 [NOAH-1::mCH(int)]) I; dpy-19(e1259) lin-12(n137) III
UP4047	noah-1(mc68 [NOAH-1::mCH(int)]) I; muls28

692

693

Figures

Figure 1. Introduction to vulva development

A) Cartoon of early L3 larva, indicating the six Vulva Precursor Cells (VPCs) beneath the somatic gonad. B) Vulva lineages and cell types. An EGF-like signal from the gonadal anchor cell (AC) induces the primary (1°) cell fate in the nearest VPC (black), which then expresses DSL ligands to induce the secondary (2°) cell fate in the adjacent VPCs (grey). The 1° and 2° VPCs divide to generate a total of twenty-two descendants of seven different cell types. C) Cartoon of mid L4 larva, showing the vulva lumen. D) L4.4 stage vulva cells visualized with the membrane marker MIG-2::GFP (muls28). The twenty-two vulval cells are organized into seven stacked rings (Sharma-Kishore et al., 1999). In the standard lateral or sagittal view, anterior is to the left and ventral is down. An orthogonal XZ view shows the oblong shape of the lumen. E) 3D rendering of the L4.4 vulva lumen generated with Imaris software (BitPlane, Zurich Switzerland), based on imaging of the matrix factor FBN-1 (see Figure 3). The YZ view at right is comparable to the transverse views of the vulva seen by TEM in Figures 4B and 9C (but note that regions deeper in the Z plane are poorly resolved here). F) The adult vulva is a slit-like and cuticle-lined passageway through which eggs are laid.

Figure 2. Cell and lumen shape changes during vulva morphogenesis

Sagittal views of the central vulva lumen. Top rows show cartoons of lumen shape for each L4 sub-stage, as defined by Mok et al (Mok et al., 2015). Middle rows show corresponding DIC images. Bottom rows show confocal slices of vulva cell membranes marked by MIG-2::GFP (muls28); cells are colored according to the key at right. Confocal stacks were collected for at least three animals per stage after L4.3. Luminal core structure is faintly visible beginning at L4.2 (red arrow). At mid-L4 (“Christmas-tree stage”; (Seydoux et al., 1993)), the vulF and vulE cells together define the vulva “neck”, the vulD and vulC cells define the vulva “shoulder”, the vulB1 and vulB2 cells define the vulva “fingers”, and the vulA cells make the connection between the vulva cells and the surrounding epidermis. *vm1 sex muscles, which attach to the mature vulva between the vulC and vulD toroids (Sharma-Kishore et al., 1999). Scale bars, 5 microns.

Figure 3. A dynamic aECM fills the vulva lumen during morphogenesis

A) aECM protein schematics. Genbank accession: FBN-1a (AFN70749.1), LET-653b (CAH60755.1), NOAH-1a (CCD66686.2), LPR-3 (CAA92030.1), LET-4 (AEZ55699.1), SYM-1 (CAB43345). Full-length FBN-1::mCherry and some LET-653 fusions were expressed from transgenes; all others were expressed from the endogenous loci tagged by CRISPR-Cas9 genome editing (see Materials and Methods). B) LET-653::SfGFP (csIs64) and FBN-1::mCherry (aaals12) show complementary luminal patterns. Medial confocal slices. Arrow, luminal core. Arrowheads, sites of ventrolateral fibril attachment to vulva cells. Lines, membrane-proximal matrix over 1° cells vulE and vulF. Bracket indicates loss of FBN-1 from the lumen over 1° cells during vulva eversion (n=3/5 L4.7, 4/4 L4.8). C) NOAH-1::mCherry (mc68) labels matrix spikes that connect to LET-653-marked luminal fibrils during vulva eversion. Left column shows overlay with cell membrane marker MIG-2::GFP (muls28) (n=9 L4.7-L4.9). Right columns show overlay with LET-653::SfGFP (cs262) (n=12 L4.7-L4.9). D) Timeline of vulva morphogenesis showing dynamic matrix patterns. Each image is a single confocal slice, inverted for clarity. For each fusion, images were collected for at least three animals per stage per strain; most fusions were imaged in multiple different strains to directly compare the different patterns (as in panels B and C). Solid green underlines indicate stages with consistent and peak localization; dashed green underlines indicate stages with more variable or weak localization. Fusions shown are FBN-1::mCherry (aaals12), LET-653::SfGFP (cs262), LET-653(ZP)::SfGFP (csIs66), SfGFP::LPR-3 (cs250), NOAH-1::mCherry (mc68), mCherry::LET-4 (cs265), and SYM-1::GFP (mc85).

Figure 4. Ultrastructural features of the mid-L4 vulva aECM

A) Transverse serial thin sections of an N2 L4.4-L4.5 stage animal were analyzed by TEM. The cartoon depicts the vulva lumen in this orientation (see also Figure 1E), and lines indicate the relative locations of different panel images. B) Whole vulva view. This thin section captures a portion of the lumen and the cell borders. Vulva cells and AC/utse are pseudo-colored according to the key shown in A. Lines indicate the relative locations of different panel images, and asterisks indicate that the panel shows a region from a different thin section of the same animal. The ventral cuticle has broken during specimen processing and oval objects surrounding the specimen are *E. coli* bacteria. C) A rough granular matrix fills the dorsal lumen. D) Core structure (white arrowheads) rises above vulC and vulD, to the level of vulE. E) Ventro-lateral fibrils (white arrowheads) and the ventral edge of the luminal matrix, which has pulled away from the broken cuticle. F) The interface between vulF (red) and vulE (yellow) forms a sequestered lumen pocket where matrix accumulates (red and yellow arrowheads). vulD (green) forms another narrow lumen pocket that is densely populated with fine fibrils (green arrowhead). G) vulF cells contain large secretory vesicles (black arrows) that are open to the extracellular space and whose contents resemble the membrane-proximal matrices that line vulF and vulE (red and yellow arrowheads, respectively). H) Lateral view of the matrix lining vulE surfaces. I, J) Examples of the very protrusive surfaces of 2°-derived cells (vulD and vulB1, respectively) that interface with fibrils. J also shows the ventral-most border of the aECM, which contains a striated layer (white arrowheads) similar to that seen in epidermal cuticle (Page & Johnstone, 2007). K) A fine-grained aECM separates the AC/utse from the rougher granular matrix of the vulva lumen; this AC matrix contains numerous EVs (orange arrowheads). All scale bars are 500 nm unless otherwise indicated. See Figure 4-1 for uncolored versions of all images.

Figure 5. Ultrastructural features of the late L4 vulva aECM

A) Longitudinal slice through the vulva of an N2 L4.8-L4.9 stage animal, with orientation similar to that in confocal images. Vulva and uterine cells are pseudo-colored as in Figure 4B. Pink arrowheads indicate matrix spikes as observed with NOAH-1::mCherry (see Figure 3C). B-E) Higher magnification views of the specimen in panel A. B) Primary vulva cells are covered in a thick membrane-proximal matrix, and the dorsal-most edge of the lumen is filled with a plug of darkly-staining material. C) The membrane-proximal matrix continues over vulD and vulC, but becomes filled with dense fibrils (green arrowheads). D) Matrix spikes (pink arrowheads) extend from vulC/D into a cuticle-like matrix below. Various other fibrils (white arrowheads) are present within this ventral matrix. E) Multi-layered nascent cuticle over vulB2. Note protrusive surface of vulB2 and multi-vesicular body (MVB) within vulB1. Many MVBs are present in vulva cells at this stage. F) Longitudinal dorsoventral slice through uterine cells and the primary vulva matrix and plug of a second N2 L4.8-L4.9 stage animal. Note the numerous EVs (orange arrowheads) present within the plug. All scale bars, 1 micron. See Figure 5-1 for uncolored versions of all images.

Figure 6. Different vulva cell types produce and assemble different aECMs

A-C) Panels in left column show cartoons of vulva cell types and lumen shape at mid-L4.

Remaining columns show single confocal slices through the vulva lumen. Fusions used are

LET-653(full-length)::SfGFP (cs262), LET-653(ZP)::SfGFP (csIs66), NOAH-1::mCherry (mc68),

SfGFP::LPR-3 (cs250). At least n=8 L4s were imaged for each strain. A) In wild type animals,

full-length LET-653 predominantly labels the core and ventro-lateral fibrils, LET-653(ZP) labels

the membrane-proximal matrix over 1° cells, NOAH-1 labels membrane-proximal matrices over

2° cells (especially vulC and vulD), and LPR-3 transiently labels membrane-proximal matrices

over all cells, but then becomes concentrated over 2° cells (see also Figure 3D). B) Loss of 1°

cells in lin-12(0) (null, n137n720) mutants disrupted the luminal core and NOAH-1 localization.

Most of the NOAH-1 pattern here is intracellular. C) Loss of 2° cells in lin-12(d) (hypermorphic,

n137) mutants disrupted the luminal core and LET-653(ZP) localization.

Figure 7. Vulva aECM assembles prior to expression of MUP-4/matrillin

A) VAB-10::GFP (cas627) marked all apical membranes in the vulva throughout L4 (including 4/4 L4.1/L4.2 stage animals). B) MUP-4::GFP (upIs1) marked apical membranes beginning in late L4 (0/3 L4.4/L4.5, 3/3 L4.6/L4.7, 2/2 L4.9). FBN-1::mCherry (aaals12 or aaaEx78) is also shown. At L4.9, MUP-4 expression is particularly strong in the vulA toroid, which surrounds the vulva opening and connects to the surrounding hyp7 epidermis. The remaining FBN-1 matrix connects to vulA at the left and right sides of the lumen, as seen in the ventral view.

Figure 8. Individual aECM factors play subtle roles in vulva eversion

A) DIC images of mutant vulvas at L4.4, L4.7 and L4.9-adult molt. At least 40 L4 animals of each genotype were imaged, including at least five each of the three stages shown. Alleles used: *fbn-1(tm290)*, *let-653(cs178)* (strains UP3342 and UP3422), *let-4(mn105)*, *sym-1(mn601)*. Asterisk indicates collapsed lumen morphology in some *let-653* mutants ($n=6/22$ L4.7, see panel C). Arrowheads indicate abnormal bulges of the vulA and vulB1/B2 cells in *fbn-1* mutants ($n=9/13$ L4.9). B) A small proportion of *let-653* mutants had progeny that hatched in utero (Egl phenotype) or ruptured at the vulva within eight days of reaching adulthood. These phenotypes were rescued by transgenes expressing full-length LET-653 or just the ZP domain. *** $p<0.0001$, Fisher's exact test. C) *let-653* mutants have reduced lumen dimensions at the L4.7 stage ($n=22$). To measure lumen dimensions, the largest box possible was drawn within the 1°-generated (Box 1) and 2°-generated (Box 2) lumen spaces, as visualized by DIC. Dimensions for Box 1 did not differ significantly between genotypes (Figure 8-1), but Box2 height was somewhat reduced. This phenotype was rescued by a transgene expressing the LET-653 ZP domain. * $p=0.031$, ** $p=0.001$, WT vs. *let-653;ls[ZP]* $p=0.085$, Mann-Whitney U test. D) WT vulva eversion. Membranes were visualized with MIG-2::GFP. Compare these para-sagittal slices to sagittal slices of the same animals in Figure 2. $n=3$ per stage. E) *let-653* mutants have irregular vulva cell shapes at the onset of vulva eversion (L4.7 stage). Membranes were visualized with MIG-2::GFP. Asterisks indicate the vm1 sex muscles. Both sagittal and para-sagittal slices from confocal Z-stacks are shown. In wild type, vulva cells are symmetrical across the midline, but in *let-653* mutants, cell shape and position are mismatched ($n=3/3$; WT: $n=0/6$). No defects in vulva cell fusion were observed (Figure 8-2). F) *let-653* mutants have subtly irregular vulva cell shapes as older L4s and adults. vulE and vulF were visualized with *daf-6pro::CFP*, and vulC and vulD were visualized with *egl-17pro::CFP* (Mok et al., 2015). Both sagittal slices and Z-projections from confocal Z-stacks are shown, along with three dimensional renderings generated with Imaris (Bitplane) from those Z-stacks. In *let-653* mutants, cell shape

836 and position are variably abnormal (n=4/4, WT: 0/3). In the specimen pictured, vulE/F appear
837 less elongated along the dorsal-ventral axis and vulC/D are slightly flattened relative to WT.
838 Arrows indicate the transition zone between vulE/F and vulC/D, where an abnormal gap occurs
839 in the mutant. In the YZ view, WT primary cells form a deep U-shape as they extend toward the
840 seam cells, but let-653 primary cells form a much shallower curve.

841

Figure 9. The ZP protein LET-653 is required for proper organization and remodeling of the vulva aECM

A) *let-653(cs178)* mutants showed relatively normal patterns of FBN-1::mCherry (aaals12) localization. Arrowhead indicates exclusion of FBN-1 from the core region. Bracket indicates exclusion of FBN-1 from the 1° lumen during eversion (n=5/5). Compare to WT in Figure 3B. B) *let-653(cs178)* mutants showed normal recruitment of SfGFP::LPR-3 (cs250) and NOAH-1::mCherry (mc68) to 2° surfaces, but abnormally delayed clearance of SfGFP::LPR-3 from vulC/D. $p = 0.0445$, Fisher's exact test. C) Transverse TEM slice of a *let-653(cs178)* mutant at mid-L4 (~L4.5) stage. Compare to the WT mid-L4 specimen in Figure 4B. Fibrils are present near the AC/utse (arrow) and the core structure (arrowhead) is not well-defined, unlike in WT (see magnified images in Figure 9-1). Box indicates region magnified in C'. C') An abnormal secretory vesicle in vulF is filled with dark aggregates that match those present in the membrane-proximal matrix over vulF (red arrowhead) and vulE (yellow arrowheads). A similar matrix continues beneath the AC/utse (see also Figure 9-1). D) WT vulF vesicles and matrix for comparison. See also Figure 4G.

Figure 10. Vulva aECM structures form independently of chondroitin

A) Chondroitin mutants showed normal recruitment of LET-653(ZP)::SfGFP (csIs66) to the membrane-proximal matrix over 1° cells. Alleles used were sqv-5(n3611) (n=4) and mig-22(k141rf) (n=10). B) WT vs. mig-22(k141rf) mutants (L4.4 stage) with membrane marker MIG-2::GFP (muls28). The vulva neck region was taller and narrower in mutants compared to wild type, while the rest of the lumen was shorter and narrower (n=15, see quantification in Figure 11B). vulD cells (green) showed the most dramatic shape changes, with an increased aspect ratio (longest axis/shortest axis, $p < 0.001$, Mann Whitney two tailed U test). WT, n=26. mig-22, n=18. C) WT vs. mig-2(k141rf) mutants (L4.5 stage) with vulE/F marker daf-6pro::CFP and vulC/D marker egl-17pro::YFP (n=3). D) mig-22(k141rf) mutants assembled a well-organized, but narrow, core structure, as seen with LET-653::SfGFP (cs262) (n=8). E) mig-2(k141rf) mutants showed normal localization of LPR-3::SfGFP and NOAH-1::mCherry to apical surfaces (n=10).

Figure 11. Chondroitin and LET-653 have both lumen-expanding and lumen-constraining roles

A) Loss of *let-653* suppressed the *mig-22(rf)* Sqv phenotype and caused over-inflation of the dorsal lumen (n=28). Alleles used were *let-653(cs178)* and *mig-22(k141rf)*. B) Lumen dimensions at the L4.4 stage were quantified as indicated in panel A. *let-653* single mutant dimensions appeared similar to wild type at this stage (n=26; see Figure 8-1). p values derived from Mann-Whitney U test; **p<0.01, ***p<0.0001. Box 1 height, *mig-22* vs. *mig-22; let-653* p=0.002. Box 1 width, *mig-22* vs. *mig-22; let-653* p=0.001. Box 2 height, *mig-22* vs. *mig-22; let-653* p=0.003. C) At late L4 stages, some *let-653* single mutants (n=3/16) and *mig-22(rf); let-653* double mutants (n=5/22) had disorganized material within the vulva lumen (line). D) Two independently generated *mig-22(rf); let-653* double mutant strains were analyzed, and both were severely egg-laying defective. ***p<0.0001, Fisher's exact test.

Figure 12. Model for aECM-dependent shaping of the vulva lumen during morphogenesis

A) The vulva lumen is initially expanded by chondroitin proteoglycans (pink arrows). Black; cuticle. Gray; apical membrane. B) A membrane-proximal aECM appears alongside matrix fibrils and a central core to halt and/or stabilize vulva expansion. vulE/F aECM; red. vulC/D aECM; green. vulA/B aECM; blue. C) The lumen narrows in the anterior-posterior axis. We propose that the central core and fibrils attach to the aECM and underlying membranes and pull ventrally, anteriorly, and posteriorly to shape the vulva lumen. The aECM changes over time; transient components turn over and the membrane-proximal matrix develops cuticle-like features. D) By adulthood, the lumen narrows into a slit and is lined by cuticle.

Supplemental Material

Figure 4 – figure supplement 1. Ultrastructural features of the mid-L4 vulva aECM

Uncolored images from Figure 4 are shown.

Figure 5 - figure supplement 1. Ultrastructural features of the late L4 vulva aECM

Uncolored images from Figure 5 are shown.

Figure 8 - figure supplement 1. Measurements of let-653, mig-22, and LET-653+ vulvas

Lumen dimensions at the L4.4 and L4.7 stages were quantified as in Figures 8 and 11.

*** $p < 0.0001$, Mann-Whitney U test. All p values between 0.01 and 0.0001 are reported. p values above 0.01 are not indicated. All measurements were performed by a researcher blinded to genotype. let-653 mutants had approximately wild-type vulvas at L4.4 stage but slightly misshapen vulvas by L4.7 stage. Overexpression of LET-653 caused expanded vulvas in a let-653 mutant background, but not in a WT background, possibly due to lower expression levels.

Figure 8 - figure supplement 2. let-653 mutant vulvas have normal cell fusion

L4.4 stage WT and let-653(cs178) vulvas with the apical junction marker DLG-1::GFP (mc103). A-A') In WT, vulA, vulC, vulD, and vulF have fused to form toroids by this stage. B-B') let-653 mutants show the same pattern of vulva cell fusion and general junction arrangement as WT. Images are maximum Z-projections of confocal Z-stacks.

Figure 9 - figure supplement 1. Vulva aECM organization differs between let-653 mutants and WT

A) let-653(cs178) mid-L4 TEM specimen from Fig. 9C. Boxes indicate regions enlarged in A' and A". A') Fibrillar structures (arrows) are present in the dorsal part of the vulva lumen near the AC/utse. A") The luminal core structure (arrowheads) is ill-defined and interspersed with various aggregates or short fibrils. B) Wildtype N2 mid-L4 TEM specimen from Figure 4. Boxes indicate regions enlarged in B' and B". B') No fibrils are detectable in the dorsal part of the vulva lumen. B") The luminal core structure is clearly defined and surrounded by a granular matrix.

929 **Source Data Files**

930 **Figure 8 – source data 1. Percentage of WT and mutants *C. elegans* that fail to lay eggs.**

931 *C. elegans* were monitored during their first week of adulthood for failure to lay eggs or rupture
932 through their vulva. Both defects were rare in WT but were more common in *let-653*, *mig-22*,
933 and *mig-22;let-653* mutants. See Figures 8 and 11.

934

935 **Figure 8 – source data 2. Measurements of WT and mutant L4.7 stage vulvas.**

936 Measurements are taken from boxes drawn within DIC images of vulvas at L4.7 stage. See
937 Figure 8 and Figure 8-1.

938

939 **Figure 10 – source data 1. Shape description of WT and *mig-22* vulD cells.**

940 The vulD cells of WT or *mig-22* L4.4 stage vulvas were traced from a single confocal slice using
941 signal from MIG-2::GFP. Shape descriptors, including aspect ratio, were calculated from these
942 tracings. See Figure 10.

943

944 **Figure 11 – source data 1. Measurements of WT and mutant L4.4 stage vulvas.**

945 Measurements are taken from boxes drawn within DIC images of vulvas at L4.4 stage. See
946 Figure 11 and Figure 8-1.

947

Key Resources Table				
Reagent type (species) or resource	Designation	Source or reference	Identifiers	Additional information
Gene (Caenorhabditis elegans)	fbn-1 III	Wormbase WS277	fbn-1; ZK783.1	FiBrilliN homolog
Gene (C. elegans)	let-653 IV	Wormbase WS277	let-653; C29E6.1	LEThal; ZP domain
Gene (C. elegans)	let-4 X	Wormbase WS277	let-4; C44H4.2	LEThal; eLRRon
Gene (C. elegans)	lin-12 III	Wormbase WS277	lin-12; R107.8	abnormal cell LINeage; Notch-related
Gene (C. elegans)	mig-22 III	Wormbase WS277	mig-22; PAR2.4	abnormal cell MIGration; chondroitin polymerizing factor
Gene (C. elegans)	mup-4 III	Wormbase WS277	mup-4; K07D8.1	MUScle Positioning; matrilin-related
Gene (C. elegans)	noah-1 I	Wormbase WS277	noah-1; C34G6.6	NOmpA homolog; ZP domain
Gene (C. elegans)	sqv-5 I	Wormbase WS277	sqv-5; T24D1.1	SQUashed Vulva; chondroitin sulfate synthase
Gene (C. elegans)	sym-1 X	Wormbase WS277	sym-1; C44H4.3	SYNthetic lethal with Mec; eLRRon
Gene (C. elegans)	vab-10 I	Wormbase WS277	vab-10; ZK1151.1	VAriaBle abnormal morphology; dystonin ortholog

Genetic reagent (<i>C. elegans</i>)	fbn-1 (tm290) III	(Kelley et al., 2015)	strain ARF335	604bp deletion/ frameshift; presumed null
Genetic reagent (<i>C. elegans</i>)	let-4 (mn105) X	(Mancuso et al., 2012)	strain UP3939	Q305ochre; presumed null
Genetic reagent (<i>C. elegans</i>)	let-4(cs265 [mCherry:: LET-4]) X	This study	strain UP3756	mCherry fused to endogenous LET-4 near its N-terminus by Cas9-triggered homologous recombination
Genetic reagent (<i>C. elegans</i>)	let-653 (cs178) IV	(Gill et al., 2016)	strain UP3244	C54ochre; presumed null
Genetic reagent (<i>C. elegans</i>)	let-653(cs262 [LET-653:: SfGFP]) IV	This study	strain UP3746	SfGFP fused to endogenous LET-653 at its C-terminus by Cas9-triggered homologous recombination
Genetic reagent (<i>C. elegans</i>)	lin-12 (n137n720) III	(Sternberg & Horvitz, 1989). Caenorhabditis Genetics Center (CGC).	strain MT2343	presumed null
Genetic reagent (<i>C. elegans</i>)	lin-12 (n137) III	(Greenwald et al., 1983). CGC.	strain MT2343	S872F; hypermorph
Genetic reagent (<i>C. elegans</i>)	lpr-3(cs250 [SfGFP:: LPR-3]) X	This study	strain UP3666	SfGFP fused to endogenous LPR-3 near its N-terminus by Cas9-triggered homologous recombination
Genetic reagent (<i>C. elegans</i>)	mig-22(k141) III	(Suzuki et al., 2006). CGC.	strain NF68	G227E; hypomorph
Genetic reagent (<i>C. elegans</i>)	noah-1(mc68 [NOAH-1:: mCherry]) I	(Vuong- Brender et al., 2017). Michel Labouesse lab.	strain ML2482	mCherry fused to endogenous NOAH-1 at internal site by Cas9-triggered

				homologous recombination
Genetic reagent (C. elegans)	sqv-5(n3611) I	(Hwang, Olson, Esko, et al., 2003). CGC.	strain MT10996	deletion; presumed null
Genetic reagent (C. elegans)	sym-1 (mn601) X	(Davies et al., 1999). CGC.	strain SP2163	Q275ochre; presumed null
Genetic reagent (C. elegans)	sym-1(mc85 [SYM-1::GFP]) X	(Vuong-Brender et al., 2017). Michel Labouesse lab.	strain ML2547	GFP fused to endogenous SYM-1 at its C-terminus by Cas9-triggered homologous recombination
Genetic reagent (C. elegans)	vab-10 (cas602 [VAB-10a::GFP])	(Yang et al., 2017). CGC.	strain GOU2043	GFP fused to endogenous VAB-10a at its C-terminus by Cas9-triggered homologous recombination
Genetic reagent - Transgene (C. elegans)	aaals12 [fbn-1pro::FBN-1::mCherry; ttx-3pro::GFP]	This study	aaals12, strain ARF379	Transgene expressing full-length FBN-1 tagged internally with mCherry inserted just prior to the ZP domain
Genetic reagent - Transgene (C. elegans)	csEx766 [lin-48pro::LET-653::SfGFP; myo-2pro::GFP]	(Forman-Rubinsky et al., 2017)	csEx766 strain UP3342	Duct-specific rescue transgene
Genetic reagent - Transgene (C. elegans)	csEx819 [grl-2pro::LET-4; myo-2p::mRFP]	(Forman-Rubinsky et al., 2017)	csEx819 strain UP3939	Duct/pore-specific rescue transgene

Genetic reagent - Transgene (C. elegans)	csIs64 [let-653pro:: SfGFP; lin-48pro:: mRFP]	(Gill et al., 2016)	csIs64 strain UP3070	Transgene expressing SfGFP-tagged LET-653
Genetic reagent - Transgene (C. elegans)	csIs66 [let-653pro:: SfGFP:: LET-653(ZP); let-653pro:: PH::mCherry; lin-48pro:: mRFP]	(Cohen, Flatt, Schroeder, & Sundaram, 2019)	csIs66 strain UP3422	Transgene expressing SfGFP-tagged LET-653(ZP) domain
Genetic reagent - Transgene (C. elegans)	mfls4[egl-17pro::YFP; daf-6pro::CFP; unc-119+]	(Félix, 2007). CGC.	mfls4 strain JU486	Transgene expressing CFP in primary vulva descendants and YFP in secondary vulva descendants.
Genetic reagent - Transgene (C. elegans)	muls28 [mig-2pro:: MIG-2::GFP; unc-31+]	(Honigberg & Kenyon, 2000). CGC.	muls28 strain CF693	Transgene expressing GFP-tagged MIG-2 (membrane marker)
Genetic reagent - Transgene (C. elegans)	upls1 [mup-4::GFP + rol-6(su1006)]	(Hong et al., 2001). CGC.	upls1; strain EE86	Transgene expressing GFP-tagged MUP-4
recombinant DNA reagent	pDD282 (plasmid)	(Dickinson et al., 2013)	Addgene plasmid #66823	GFP ⁺ SEC ⁺ 3xFlag vector with ccdB markers for cloning homology arms
recombinant DNA reagent	pDD162 (plasmid)	(Dickinson et al., 2013)	Addgene plasmid #47549	eft-3p::Cas9 + empty sgRNA plasmid
recombinant DNA reagent	pJC39	This study		pDD282 with GFP replaced by SfGFP
recombinant DNA reagent	pJC49	This study		let-653 homology repair template generated by PCR with OJC201+OJC202

				and oJC203+oJC204 and cloned into pJC39
recombinant DNA reagent	pJC50	This study		let-653 sgRNA sequence (5'- TTGAGATATTAC GTTCGAAC-3') cloned into pDD162
recombinant DNA reagent	pJC67	This study		let-4 homology repair template generated by PCR with oJC269+oJC270 and oJC271+oJC282 and cloned into pMLS291
recombinant DNA reagent	pJC68	This study		let-4 sgRNA sequence (5'- GACTCCAGGACA AGCATTTG -3') cloned into pDD162
recombinant DNA reagent	pMLS291 (plasmid)	(Schwartz & Jorgensen, 2016)	Addgene plasmid #73724	SapTrap vector with mCherry
recombinant DNA reagent	pMLS328 (plasmid)	(Schwartz & Jorgensen, 2016)	Addgene plasmid #73717	eft-3p::2xNLS- Cre, unc-119+, for SEC excision
recombinant DNA reagent	pRFR60	This study		lpr-3 sgRNA sequence (5'- TTTGGCTACG ACGTTAGCTG -3') cloned into pDD162
recombinant DNA reagent	pRFR70	This study		lpr-3 homology repair template generated by PCR with oRFR69+oRFR9 0 and oRFR71+oRFR7 2 and cloned into pJC39

sequence-based reagent	oJC201	This study	PCR primer	5'_ACGTTGTAAA ACGACGGCCAGT CGCCGGCA- CAAAAATCAGTC TATCATTCC_3'
sequence-based reagent	oJC202	This study	PCR primer	5'_TCCAGTGAAA AGTTCTTCTCCTT TGCTGAT- GATGTTTgCAGTT CGAACG_3'
sequence-based reagent	oJC203	This study	PCR primer	5'_CGTGATTACA AGGATGACGATG ACAAGAGA- TGAAAATACACA CAAAAAATG_3'
sequence-based reagent	oJC204	This study	PCR primer	5'_TCACACAGGA AACAGCTATGAC CATGTTAT- GTCTGGTAGCTG CTTTGATGATGG _3'
sequence-based reagent	oJC269	This study	PCR primer	5'_GTGGCTCTTC GTGGGTTTAAAC ACGTATTTCA CATTTCAG_3'
sequence-based reagent	oJC270	This study	PCR primer	5'_GTGGCTCTTC GCATTCCAGGAC AAGCATTTGT <u>C</u> AG_3'
sequence-based reagent	oJC271	This study	PCR primer	5'_GTGGCTCTTC GGGTGTCATTAC TCAAGC <u>G</u> TGCTT C_3'
sequence-based reagent	oJC282	This study	PCR primer	5'_GTGGCTCTTC gTACGATGGCAC TGCAGTCATATT G_3'
sequence-based reagent	oRFR69	This study	PCR primer	5'_ACGTTGTAAA ACGACGGCCAGT CGCCGGCACATA

				TAATAAAGCATTT TGTCTG_3'
sequence-based reagent	oRFR90	This study	PCR primer	5'_TCCAGTGAAA AGTTCTTCTCCTT TGCTgATGCCTA GTGCgACAGCTA AC_3'
sequence-based reagent	oRFR71	This study	PCR primer	5'_CGTGATTACA AGGATGACGATG ACAAGAGAGCTA TTAGCGAAGCAG ACGTACC_3'
sequence-based reagent	oRFR72	This study	PCR primer	5'_TCACACAGGA AACAGCTATGAC CATGTTATCGGT AACGGTCTTGAC TCCGGC_3'
software, algorithm	ImageJ	NIH		
software, algorithm	Adobe Illustrator	Adobe		
software, algorithm	Imaris	Bitplane		
software, algorithm	Prism	Graphpad		

949

950

References

- Andrew, D. J., & Ewald, A. J. (2010). Morphogenesis of epithelial tubes: Insights into tube formation, elongation, and elaboration. *Dev Biol*, 341(1), 34-55. doi:10.1016/j.ydbio.2009.09.024
- Bagnat, M., Cheung, I. D., Mostov, K. E., & Stainier, D. Y. (2007). Genetic control of single lumen formation in the zebrafish gut. *Nat Cell Biol*, 9(8), 954-960. doi:10.1038/ncb1621
- Bender, A. M., Kirienko, N. V., Olson, S. K., Esko, J. D., & Fay, D. S. (2007). lin-35/Rb and the CoREST ortholog spr-1 coordinately regulate vulval morphogenesis and gonad development in *C. elegans*. *Dev Biol*, 302(2), 448-462. doi:10.1016/j.ydbio.2006.09.051
- Bercher, M., Wahl, J., Vogel, B. E., Lu, C., Hedgecock, E. M., Hall, D. H., & Plenefisch, J. D. (2001). mua-3, a gene required for mechanical tissue integrity in *Caenorhabditis elegans*, encodes a novel transmembrane protein of epithelial attachment complexes. *J Cell Biol*, 154(2), 415-426. doi:10.1083/jcb.200103035
- Bernhard, W. (2016). Lung surfactant: Function and composition in the context of development and respiratory physiology. *Ann Anat*, 208, 146-150. doi:10.1016/j.aanat.2016.08.003
- Birchenough, G. M., Johansson, M. E., Gustafsson, J. K., Bergström, J. H., & Hansson, G. C. (2015). New developments in goblet cell mucus secretion and function. *Mucosal Immunol*, 8(4), 712-719. doi:10.1038/mi.2015.32
- Bokhove, M., & Jovine, L. (2018). Structure of Zona Pellucida Module Proteins. *Curr Top Dev Biol*, 130, 413-442. doi:10.1016/bs.ctdb.2018.02.007
- Bosher, J. M., Hahn, B. S., Legouis, R., Sookhareea, S., Weimer, R. M., Gansmuller, A., . . . Labouesse, M. (2003). The *Caenorhabditis elegans* vab-10 spectraplakins isoforms protect the epidermis against internal and external forces. *J Cell Biol*, 161(4), 757-768. doi:10.1083/jcb.200302151
- Brenner, S. (1974). The genetics of *Caenorhabditis elegans*. *Genetics*, 77(1), 71-94.
- Chappell, D., Jacob, M., Paul, O., Rehm, M., Welsch, U., Stoeckelhuber, M., . . . Becker, B. F. (2009). The glycocalyx of the human umbilical vein endothelial cell: an impressive structure ex vivo but not in culture. *Circ Res*, 104(11), 1313-1317. doi:10.1161/circresaha.108.187831
- Cohen, J. D., Flatt, K. M., Schroeder, N. E., & Sundaram, M. V. (2019). Epithelial Shaping by Diverse Apical Extracellular Matrices Requires the Nidogen Domain Protein DEX-1 in *Caenorhabditis elegans*. *Genetics*, 211(1), 185-200. doi:10.1534/genetics.118.301752
- Davies, A. G., Spike, C. A., Shaw, J. E., & Herman, R. K. (1999). Functional overlap between the mec-8 gene and five sym genes in *Caenorhabditis elegans*. *Genetics*, 153(1), 117-134.
- Devine, W. P., Lubarsky, B., Shaw, K., Luschnig, S., Messina, L., & Krasnow, M. A. (2005). Requirement for chitin biosynthesis in epithelial tube morphogenesis. *Proc Natl Acad Sci U S A*, 102(47), 17014-17019. doi:10.1073/pnas.0506676102
- Dickinson, D. J., Pani, A. M., Heppert, J. K., Higgins, C. D., & Goldstein, B. (2015). Streamlined Genome Engineering with a Self-Excising Drug Selection Cassette. *Genetics*, 200(4), 1035-1049. doi:10.1534/genetics.115.178335
- Dickinson, D. J., Ward, J. D., Reiner, D. J., & Goldstein, B. (2013). Engineering the *Caenorhabditis elegans* genome using Cas9-triggered homologous recombination. *Nat Methods*, 10(10), 1028-1034. doi:10.1038/nmeth.2641
- Dodt, H. U., & Ziegler, W. (1990). Visualizing unstained neurons in living brain slices by infrared DIC-videomicroscopy. *Brain Res*, 537(1-2), 333-336. doi:10.1016/0006-8993(90)90380-t
- Dong, B., Deng, W., & Jiang, D. (2011). Distinct cytoskeleton populations and extensive crosstalk control Ciona notochord tubulogenesis. *Development*, 138(8), 1631-1641. doi:10.1242/dev.057208
- Farooqui, S., Pellegrino, M. W., Rimann, I., Morf, M. K., Müller, L., Fröhli, E., & Hajnal, A. (2012). Coordinated lumen contraction and expansion during vulval tube morphogenesis in *Caenorhabditis elegans*. *Dev Cell*, 23(3), 494-506. doi:10.1016/j.devcel.2012.06.019

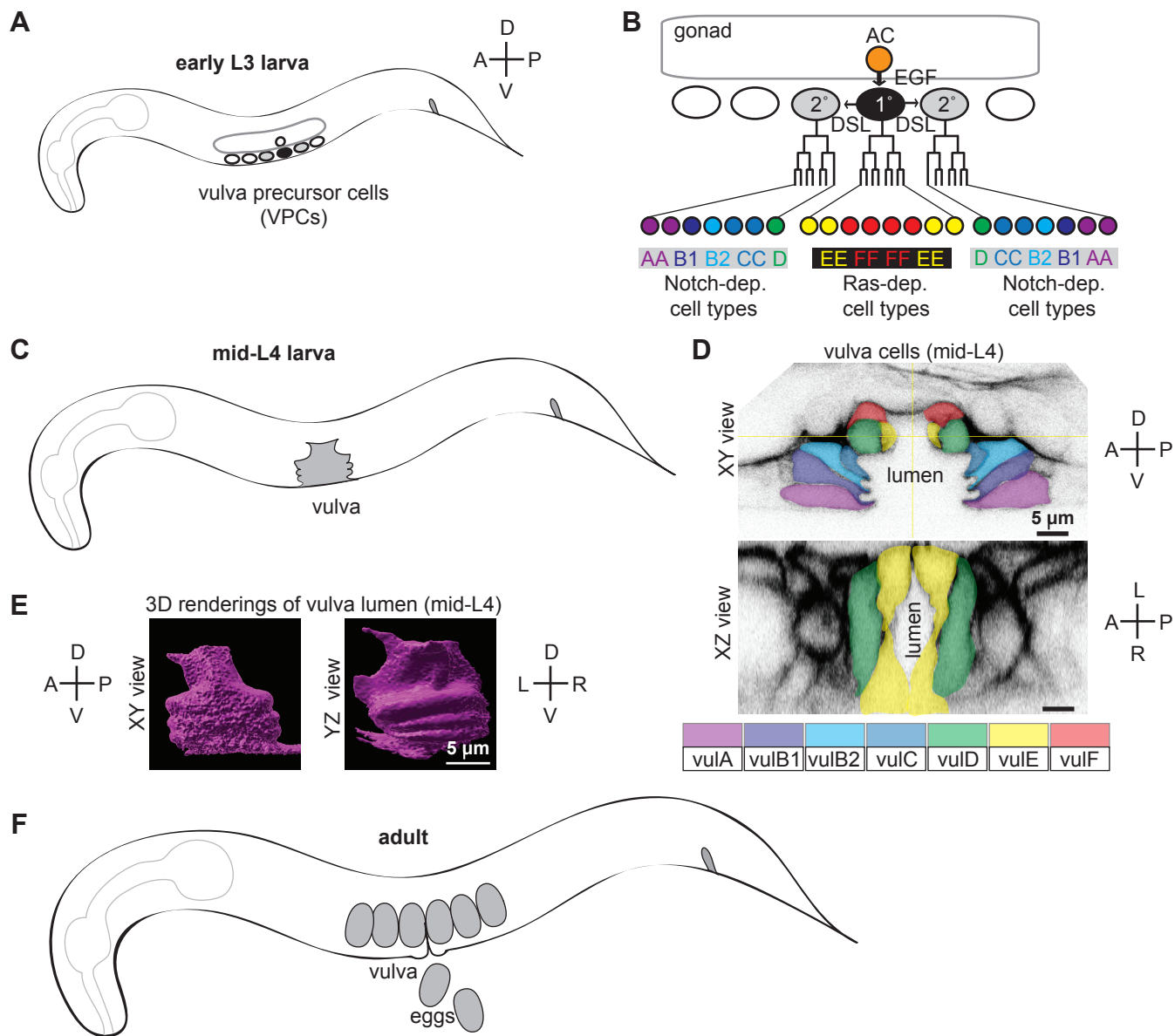
998 Félix, M. A. (2007). Cryptic quantitative evolution of the vulva intercellular signaling network in
 999 *Caenorhabditis*. *Curr Biol*, 17(2), 103-114. doi:10.1016/j.cub.2006.12.024
 1000 Fletcher, D. A., & Mullins, R. D. (2010). Cell mechanics and the cytoskeleton. *Nature*, 463(7280), 485-
 1001 492. doi:10.1038/nature08908
 1002 Forman-Rubinsky, R., Cohen, J. D., & Sundaram, M. V. (2017). Lipocalins Are Required for Apical
 1003 Extracellular Matrix Organization and Remodeling in *Caenorhabditis elegans*. *Genetics*, 207(2),
 1004 625-642. doi:10.1534/genetics.117.300207
 1005 Gill, H. K., Cohen, J. D., Ayala-Figueroa, J., Forman-Rubinsky, R., Poggioli, C., Bickard, K., . . . Sundaram,
 1006 M. V. (2016). Integrity of Narrow Epithelial Tubes in the *C. elegans* Excretory System Requires a
 1007 Transient Luminal Matrix. *PLoS Genet*, 12(8), e1006205. doi:10.1371/journal.pgen.1006205
 1008 Greenwald, I. S., Sternberg, P. W., & Horvitz, H. R. (1983). The *lin-12* locus specifies cell fates in
 1009 *Caenorhabditis elegans*. *Cell*, 34(2), 435-444. doi:10.1016/0092-8674(83)90377-x
 1010 Gupta, B. P., Hanna-Rose, W., & Sternberg, P. W. (2012). Morphogenesis of the vulva and the vulval-
 1011 uterine connection. *WormBook*, 1-20. doi:10.1895/wormbook.1.152.1
 1012 Hall, D. H., Hartweg, E., & Nguyen, K. C. (2012). Modern electron microscopy methods for *C. elegans*.
 1013 *Methods Cell Biol*, 107, 93-149. doi:10.1016/b978-0-12-394620-1.00004-7
 1014 Herman, T., Hartweg, E., & Horvitz, H. R. (1999). *sqv* mutants of *Caenorhabditis elegans* are defective in
 1015 vulval epithelial invagination. *Proc Natl Acad Sci U S A*, 96(3), 968-973.
 1016 doi:10.1073/pnas.96.3.968
 1017 Hill, R. J., & Sternberg, P. W. (1992). The gene *lin-3* encodes an inductive signal for vulval development in
 1018 *C. elegans*. *Nature*, 358(6386), 470-476. doi:10.1038/358470a0
 1019 Holmes, D. F., Lu, Y., Starborg, T., & Kadler, K. E. (2018). Collagen Fibril Assembly and Function. *Curr Top*
 1020 *Dev Biol*, 130, 107-142. doi:10.1016/bs.ctdb.2018.02.004
 1021 Hong, L., Elbl, T., Ward, J., Franzini-Armstrong, C., Rybicka, K. K., Gatewood, B. K., . . . Bucher, E. A.
 1022 (2001). MUP-4 is a novel transmembrane protein with functions in epithelial cell adhesion in
 1023 *Caenorhabditis elegans*. *J Cell Biol*, 154(2), 403-414. doi:10.1083/jcb.200007075
 1024 Honigberg, L., & Kenyon, C. (2000). Establishment of left/right asymmetry in neuroblast migration by
 1025 UNC-40/DCC, UNC-73/Trio and DPY-19 proteins in *C. elegans*. *Development*, 127(21), 4655-4668.
 1026 Hwang, H. Y., & Horvitz, H. R. (2002a). The *Caenorhabditis elegans* vulval morphogenesis gene *sqv-4*
 1027 encodes a UDP-glucose dehydrogenase that is temporally and spatially regulated. *Proc Natl*
 1028 *Acad Sci U S A*, 99(22), 14224-14229. doi:10.1073/pnas.172522499
 1029 Hwang, H. Y., & Horvitz, H. R. (2002b). The SQV-1 UDP-glucuronic acid decarboxylase and the SQV-7
 1030 nucleotide-sugar transporter may act in the Golgi apparatus to affect *Caenorhabditis elegans*
 1031 vulval morphogenesis and embryonic development. *Proc Natl Acad Sci U S A*, 99(22), 14218-
 1032 14223. doi:10.1073/pnas.172522199
 1033 Hwang, H. Y., Olson, S. K., Brown, J. R., Esko, J. D., & Horvitz, H. R. (2003). The *Caenorhabditis elegans*
 1034 genes *sqv-2* and *sqv-6*, which are required for vulval morphogenesis, encode glycosaminoglycan
 1035 galactosyltransferase II and xylosyltransferase. *J Biol Chem*, 278(14), 11735-11738.
 1036 doi:10.1074/jbc.C200518200
 1037 Hwang, H. Y., Olson, S. K., Esko, J. D., & Horvitz, H. R. (2003). *Caenorhabditis elegans* early
 1038 embryogenesis and vulval morphogenesis require chondroitin biosynthesis. *Nature*, 423(6938),
 1039 439-443. doi:10.1038/nature01634
 1040 Ihara, S., Hagedorn, E. J., Morrissey, M. A., Chi, Q., Motegi, F., Kramer, J. M., & Sherwood, D. R. (2011).
 1041 Basement membrane sliding and targeted adhesion remodels tissue boundaries during uterine-
 1042 vulval attachment in *Caenorhabditis elegans*. *Nat Cell Biol*, 13(6), 641-651. doi:10.1038/ncb2233
 1043 Inoue, T., Oz, H. S., Wiland, D., Gharib, S., Deshpande, R., Hill, R. J., . . . Sternberg, P. W. (2004). *C.*
 1044 *elegans* LIN-18 is a Ryk ortholog and functions in parallel to LIN-17/Frizzled in Wnt signaling. *Cell*,
 1045 118(6), 795-806. doi:10.1016/j.cell.2004.09.001

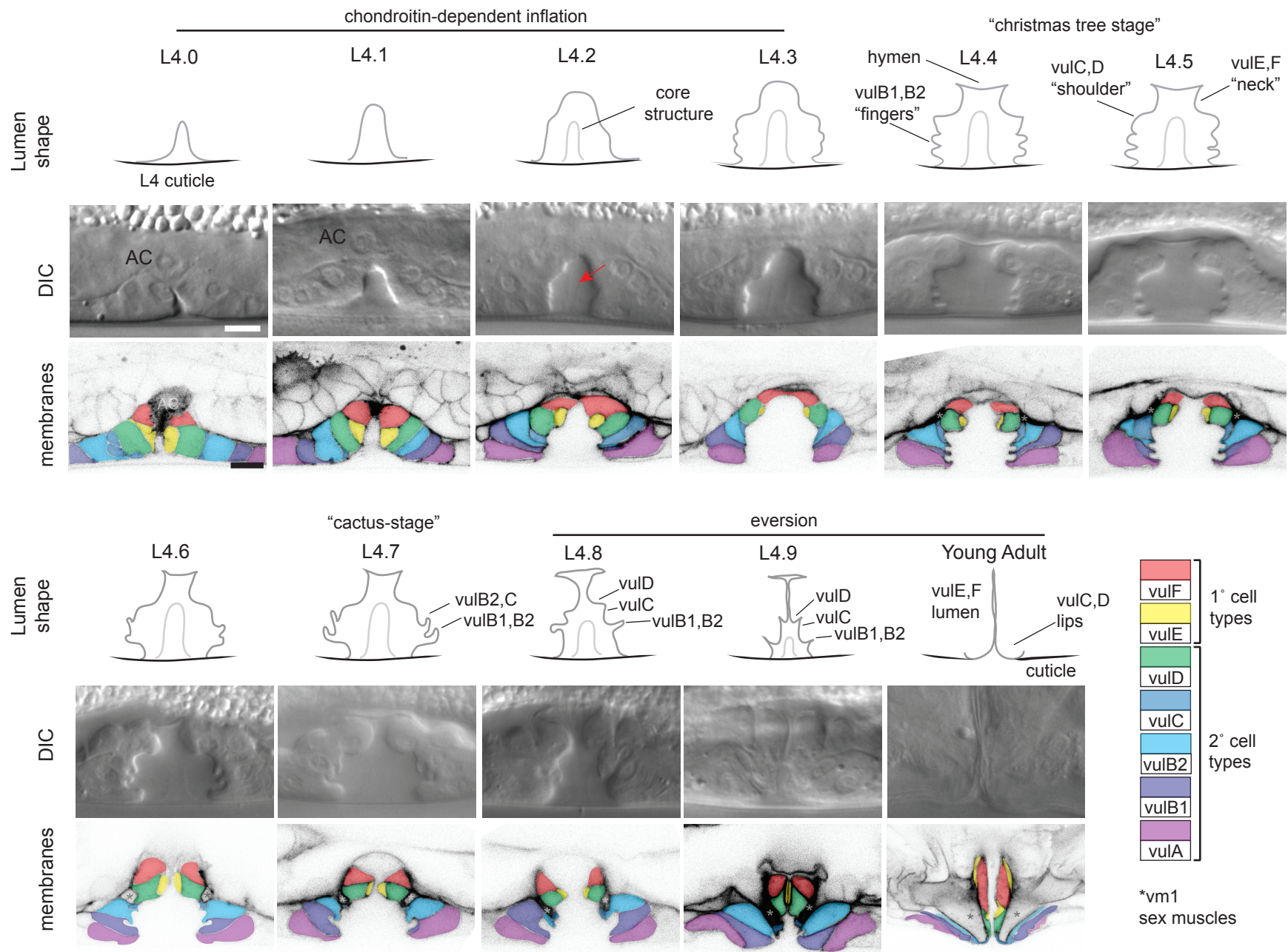
- Inoue, T., Sherwood, D. R., Aspöck, G., Butler, J. A., Gupta, B. P., Kirouac, M., . . . Sternberg, P. W. (2002). Gene expression markers for *Caenorhabditis elegans* vulval cells. *Gene Expr Patterns*, 2(3-4), 235-241. doi:10.1016/s1567-133x(02)00055-8
- Inoue, T., Wang, M., Ririe, T. O., Fernandes, J. S., & Sternberg, P. W. (2005). Transcriptional network underlying *Caenorhabditis elegans* vulval development. *Proc Natl Acad Sci U S A*, 102(14), 4972-4977. doi:10.1073/pnas.0408122102
- Izumikawa, T., Kitagawa, H., Mizuguchi, S., Nomura, K. H., Nomura, K., Tamura, J., . . . Sugahara, K. (2004). Nematode chondroitin polymerizing factor showing cell-/organ-specific expression is indispensable for chondroitin synthesis and embryonic cell division. *J Biol Chem*, 279(51), 53755-53761. doi:10.1074/jbc.M409615200
- Jazwinska, A., Ribeiro, C., & Affolter, M. (2003). Epithelial tube morphogenesis during *Drosophila* tracheal development requires Piopio, a luminal ZP protein. *Nat Cell Biol*, 5(10), 895-901. doi:10.1038/ncb1049
- Johansson, M. E., Ambort, D., Pelaseyed, T., Schutte, A., Gustafsson, J. K., Ermund, A., . . . Hansson, G. C. (2011). Composition and functional role of the mucus layers in the intestine. *Cell Mol Life Sci*, 68(22), 3635-3641. doi:10.1007/s00018-011-0822-3
- Johansson, M. E., Sjövall, H., & Hansson, G. C. (2013). The gastrointestinal mucus system in health and disease. *Nat Rev Gastroenterol Hepatol*, 10(6), 352-361. doi:10.1038/nrgastro.2013.35
- Jovine, L., Qi, H., Williams, Z., Litscher, E. S., & Wassarman, P. M. (2007). Features that affect secretion and assembly of zona pellucida glycoproteins during mammalian oogenesis. *Soc Reprod Fertil Suppl*, 63, 187-201.
- Judge, D. P., & Dietz, H. C. (2005). Marfan's syndrome. *Lancet*, 366(9501), 1965-1976. doi:10.1016/s0140-6736(05)67789-6
- Katz, S. S., Maybrun, C., Maul-Newby, H. M., & Frand, A. R. (2018). Non-canonical apical constriction shapes emergent matrices in *C. elegans*. *bioRxiv*, 189951. doi:10.1101/189951
- Kelley, M., Yochem, J., Krieg, M., Calixto, A., Heiman, M. G., Kuzmanov, A., . . . Fay, D. S. (2015). FBN-1, a fibrillin-related protein, is required for resistance of the epidermis to mechanical deformation during *C. elegans* embryogenesis. *Elife*, 4. doi:10.7554/eLife.06565
- Khan, L. A., Zhang, H., Abraham, N., Sun, L., Fleming, J. T., Buechner, M., . . . Gobel, V. (2013). Intracellular lumen extension requires ERM-1-dependent apical membrane expansion and AQP-8-mediated flux. *Nat Cell Biol*, 15(2), 143-156. doi:10.1038/ncb2656
- Kishore, R. S., & Sundaram, M. V. (2002). ced-10 Rac and mig-2 function redundantly and act with unc-73 trio to control the orientation of vulval cell divisions and migrations in *Caenorhabditis elegans*. *Dev Biol*, 241(2), 339-348. doi:10.1006/dbio.2001.0513
- Kolotuev, I., Hyenne, V., Schwab, Y., Rodriguez, D., & Labouesse, M. (2013). A pathway for unicellular tube extension depending on the lymphatic vessel determinant Prox1 and on osmoregulation. *Nat Cell Biol*, 15(2), 157-168. doi:10.1038/ncb2662
- Kreda, S. M., Davis, C. W., & Rose, M. C. (2012). CFTR, mucins, and mucus obstruction in cystic fibrosis. *Cold Spring Harb Perspect Med*, 2(9), a009589. doi:10.1101/cshperspect.a009589
- Labouesse, M. (2012). Role of the extracellular matrix in epithelial morphogenesis: a view from *C. elegans*. *Organogenesis*, 8(2), 65-70. doi:10.4161/org.20261
- Lane, M. C., Koehl, M. A., Wilt, F., & Keller, R. (1993). A role for regulated secretion of apical extracellular matrix during epithelial invagination in the sea urchin. *Development*, 117(3), 1049-1060.
- Lazetic, V., & Fay, D. S. (2017). Conserved Ankyrin Repeat Proteins and Their NIMA Kinase Partners Regulate Extracellular Matrix Remodeling and Intracellular Trafficking in *Caenorhabditis elegans*. *Genetics*, 205(1), 273-293. doi:10.1534/genetics.116.194464

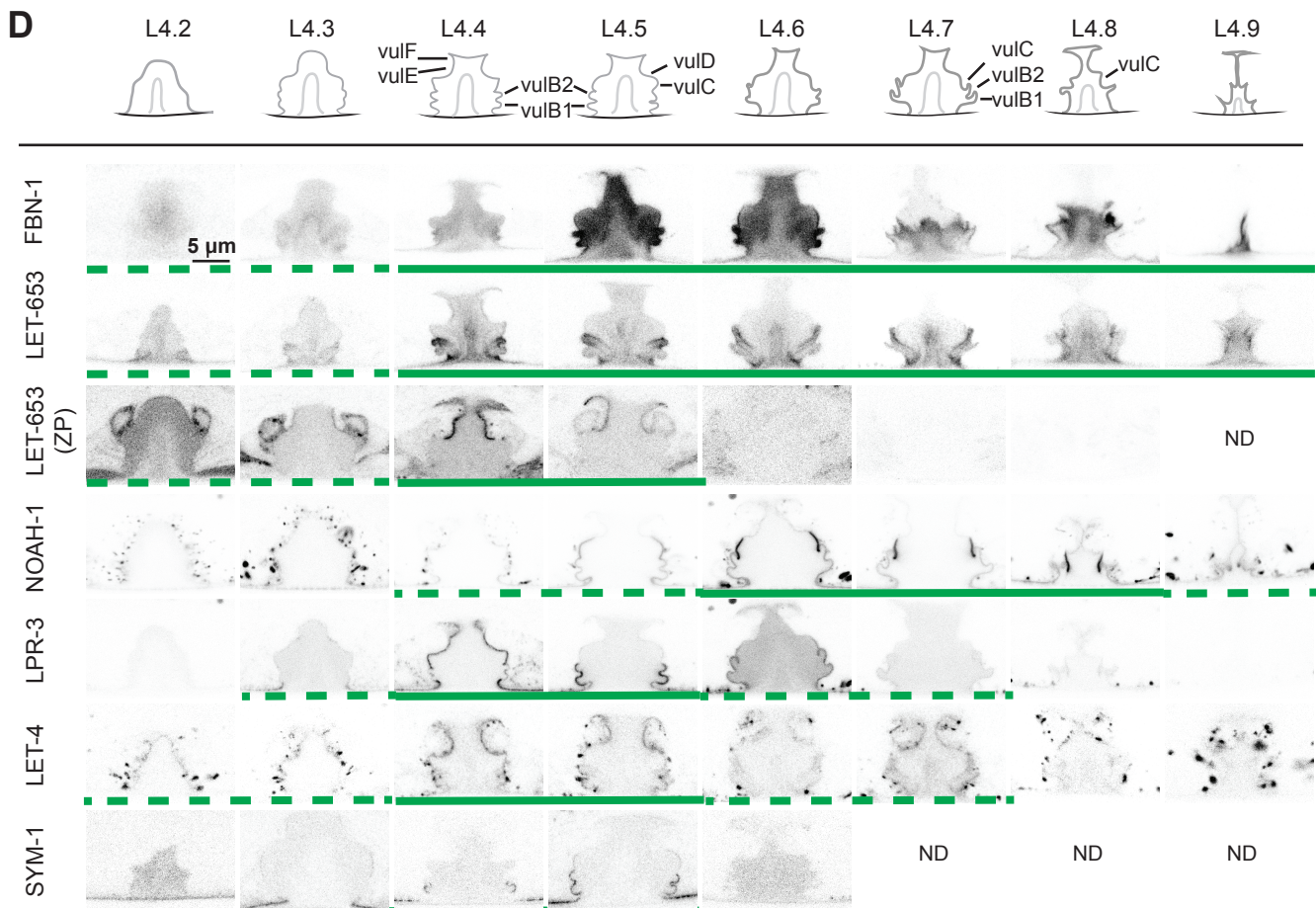
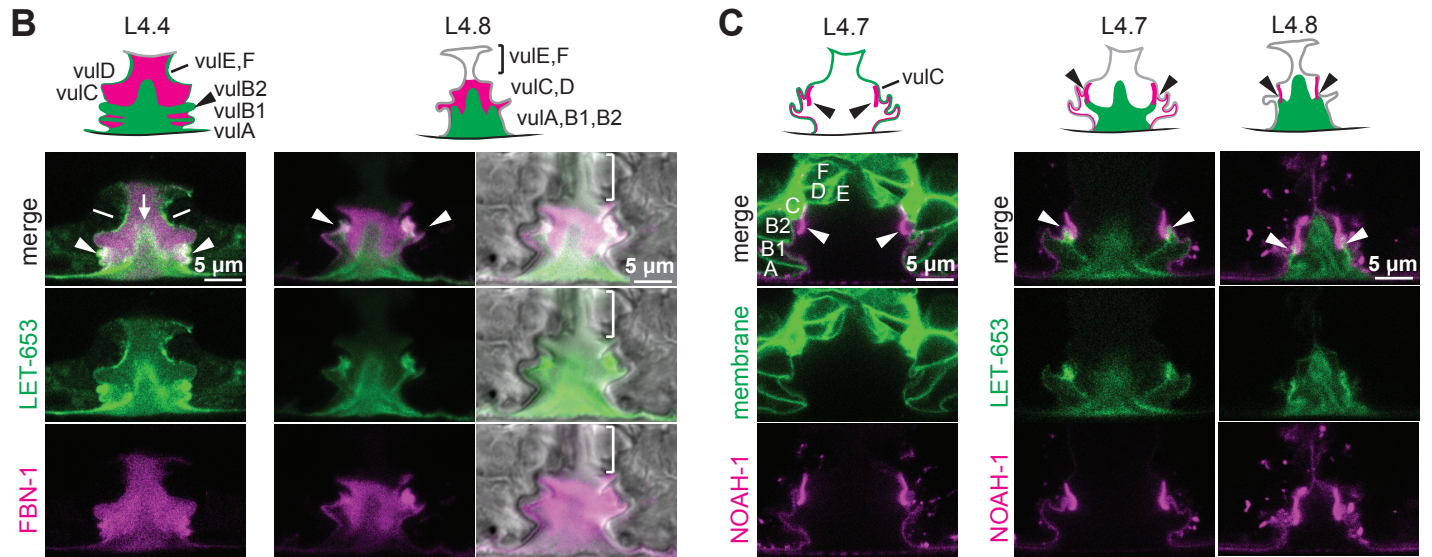
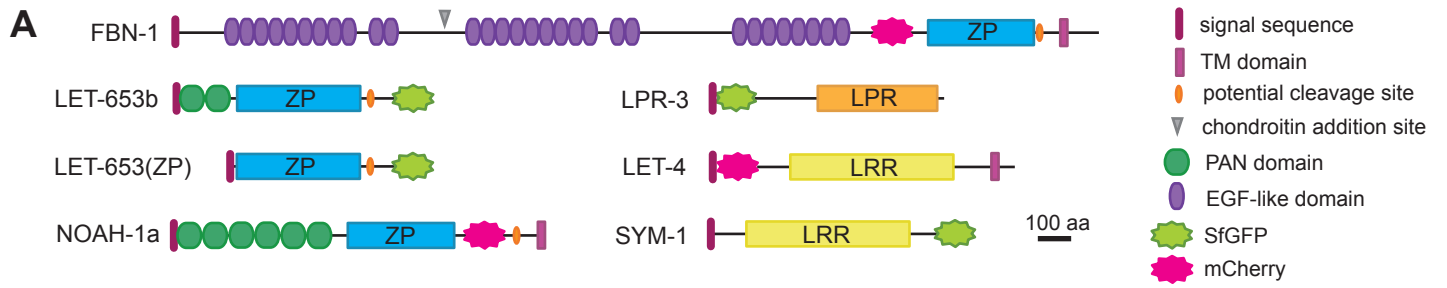
- Linde-Medina, M., & Marcucio, R. (2018). Living tissues are more than cell clusters: The extracellular matrix as a driving force in morphogenesis. *Prog Biophys Mol Biol*, 137, 46-51. doi:10.1016/j.pbiomolbio.2018.01.009
- Luschnig, S., & Uv, A. (2014). Luminal matrices: an inside view on organ morphogenesis. *Exp Cell Res*, 321(1), 64-70. doi:10.1016/j.yexcr.2013.09.010
- Malhotra, V., & Erlmann, P. (2015). The pathway of collagen secretion. *Annu Rev Cell Dev Biol*, 31, 109-124. doi:10.1146/annurev-cellbio-100913-013002
- Mancuso, V. P., Parry, J. M., Storer, L., Poggioli, C., Nguyen, K. C., Hall, D. H., & Sundaram, M. V. (2012). Extracellular leucine-rich repeat proteins are required to organize the apical extracellular matrix and maintain epithelial junction integrity in *C. elegans*. *Development*, 139(5), 979-990. doi:10.1242/dev.075135
- Matus, D. Q., Chang, E., Makohon-Moore, S. C., Hagedorn, M. A., Chi, Q., & Sherwood, D. R. (2014). Cell division and targeted cell cycle arrest opens and stabilizes basement membrane gaps. *Nat Commun*, 5, 4184. doi:10.1038/ncomms5184
- McClatchey, S. T., Wang, Z., Linden, L. M., Hastie, E. L., Wang, L., Shen, W., . . . Sherwood, D. R. (2016). Boundary cells restrict dystroglycan trafficking to control basement membrane sliding during tissue remodeling. *Elife*, 5. doi:10.7554/eLife.17218
- Mok, D. Z., Sternberg, P. W., & Inoue, T. (2015). Morphologically defined sub-stages of *C. elegans* vulval development in the fourth larval stage. *BMC Dev Biol*, 15, 26. doi:10.1186/s12861-015-0076-7
- Navis, A., Marjoram, L., & Bagnat, M. (2013). Cfr controls lumen expansion and function of Kupffer's vesicle in zebrafish. *Development*, 140(8), 1703-1712. doi:10.1242/dev.091819
- Navis, A., & Nelson, C. M. (2016). Pulling together: Tissue-generated forces that drive lumen morphogenesis. *Semin Cell Dev Biol*, 55, 139-147. doi:10.1016/j.semcdb.2016.01.002
- Niwa, R., Hada, K., Moliyama, K., Ohniwa, R. L., Tan, Y. M., Olsson-Carter, K., . . . Slack, F. J. (2009). *C. elegans* sym-1 is a downstream target of the hunchback-like-1 developmental timing transcription factor. *Cell Cycle*, 8(24), 4147-4154. doi:10.4161/cc.8.24.10292
- Noborn, F., Gomez Toledo, A., Nasir, W., Nilsson, J., Dierker, T., Kjellén, L., & Larson, G. (2018). Expanding the chondroitin glycoproteome of *Caenorhabditis elegans*. *J Biol Chem*, 293(1), 379-389. doi:10.1074/jbc.M117.807800
- Olson, S. K., Bishop, J. R., Yates, J. R., Oegema, K., & Esko, J. D. (2006). Identification of novel chondroitin proteoglycans in *Caenorhabditis elegans*: embryonic cell division depends on CPG-1 and CPG-2. *J Cell Biol*, 173(6), 985-994. doi:10.1083/jcb.200603003
- Page, A. P., & Johnstone, I. L. (2007). The cuticle. *WormBook*, 1-15. doi:10.1895/wormbook.1.138.1
- Pásti, G., & Labouesse, M. (2014). Epithelial junctions, cytoskeleton, and polarity. *WormBook*, 1-35. doi:10.1895/wormbook.1.56.2
- Perrimon, N., & Bernfield, M. (2000). Specificities of heparan sulphate proteoglycans in developmental processes. *Nature*, 404(6779), 725-728. doi:10.1038/35008000
- Plaza, S., Chanut-Delalande, H., Fernandes, I., Wassarman, P. M., & Payre, F. (2010). From A to Z: apical structures and zona pellucida-domain proteins. *Trends Cell Biol*, 20(9), 524-532. doi:10.1016/j.tcb.2010.06.002
- Priess, J. R., & Hirsh, D. I. (1986). *Caenorhabditis elegans* morphogenesis: the role of the cytoskeleton in elongation of the embryo. *Dev Biol*, 117(1), 156-173. doi:10.1016/0012-1606(86)90358-1
- Pu, P., Stone, C. E., Burdick, J. T., Murray, J. I., & Sundaram, M. V. (2017). The Lipocalin LPR-1 Cooperates with LIN-3/EGF Signaling To Maintain Narrow Tube Integrity in *Caenorhabditis elegans*. *Genetics*, 205(3), 1247-1260. doi:10.1534/genetics.116.195156
- Rosa, J. B., Metzstein, M. M., & Ghabrial, A. S. (2018). An lchor-dependent apical extracellular matrix regulates seamless tube shape and integrity. *PLoS Genet*, 14(1), e1007146. doi:10.1371/journal.pgen.1007146

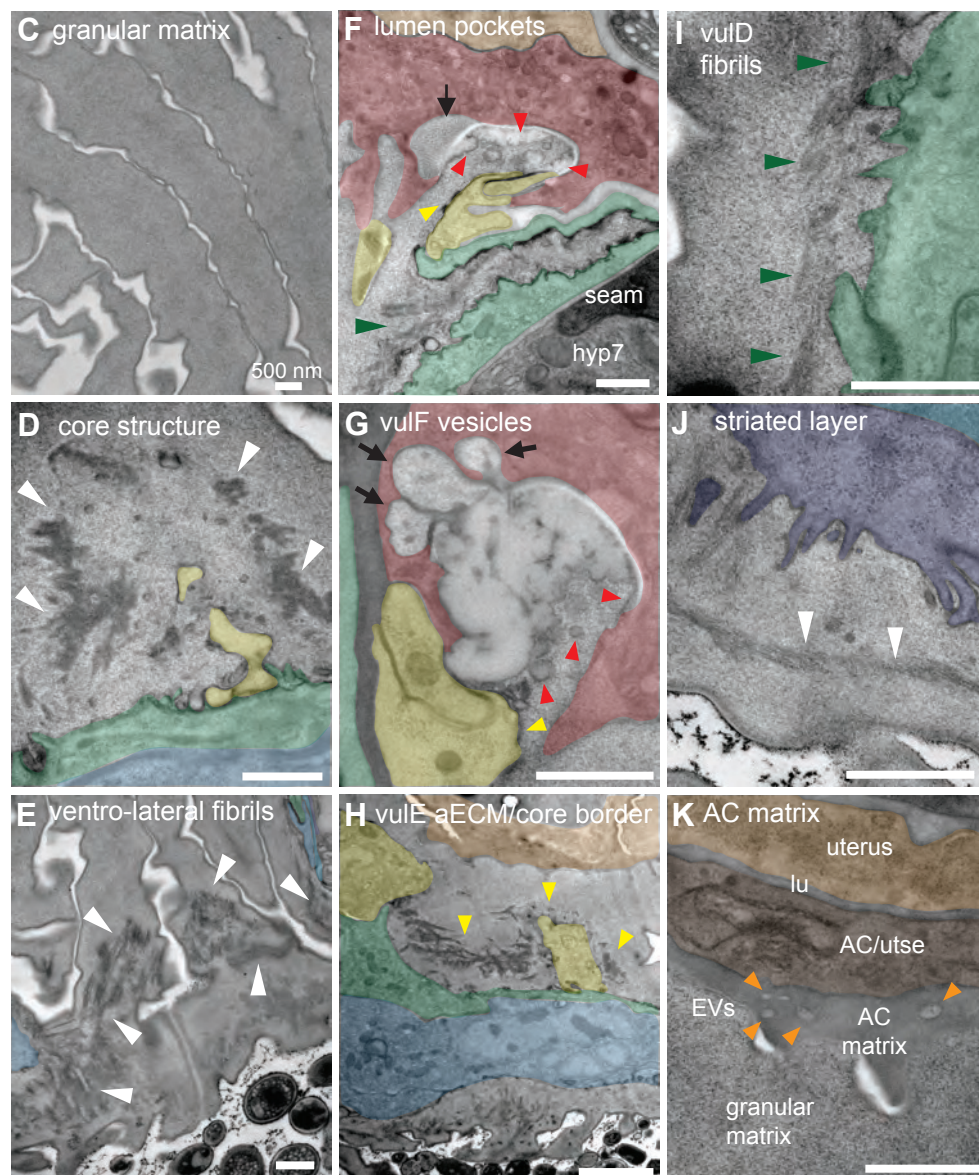
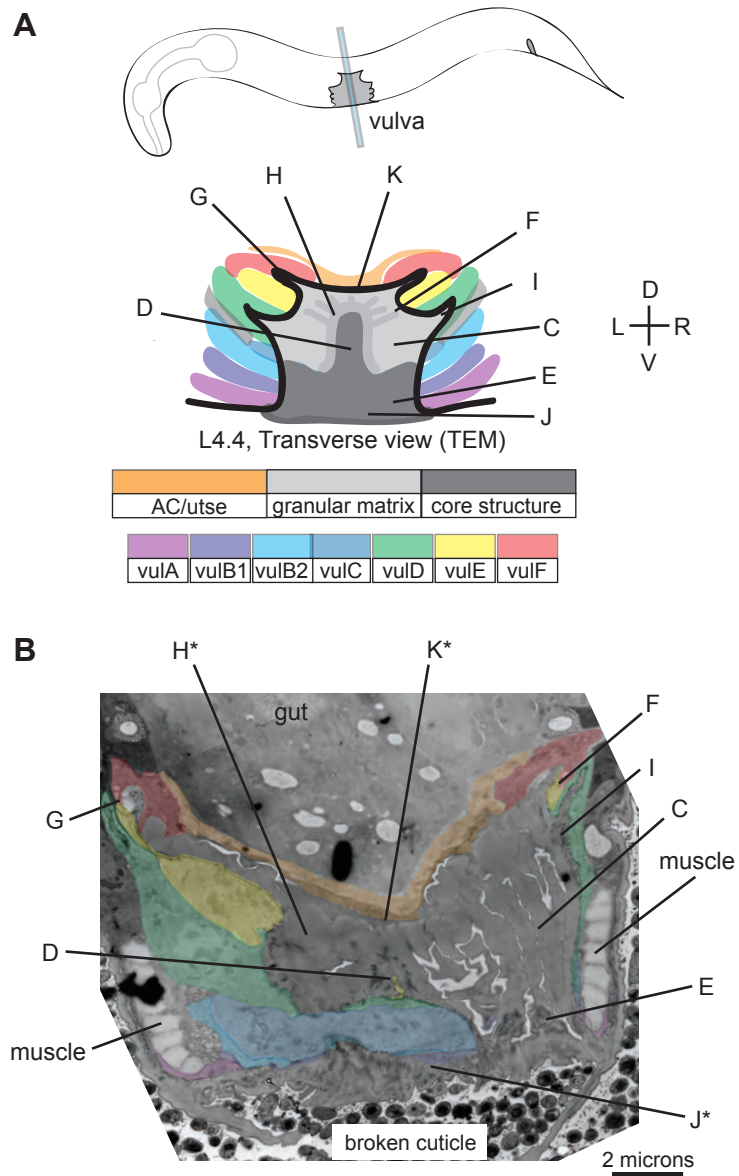
1140 Sapio, M. R., Hilliard, M. A., Cermola, M., Favre, R., & Bazzicalupo, P. (2005). The Zona Pellucida domain
 1141 containing proteins, CUT-1, CUT-3 and CUT-5, play essential roles in the development of the
 1142 larval alae in *Caenorhabditis elegans*. *Dev Biol*, 282(1), 231-245.
 1143 doi:10.1016/j.ydbio.2005.03.011
 1144 Sapir, A., Choi, J., Leikina, E., Avinoam, O., Valansi, C., Chernomordik, L. V., . . . Podbilewicz, B. (2007).
 1145 AFF-1, a FOS-1-regulated fusogen, mediates fusion of the anchor cell in *C. elegans*. *Dev Cell*,
 1146 12(5), 683-698. doi:10.1016/j.devcel.2007.03.003
 1147 Schindler, A. J., & Sherwood, D. R. (2013). Morphogenesis of the *caenorhabditis elegans* vulva. *Wiley*
 1148 *Interdiscip Rev Dev Biol*, 2(1), 75-95. doi:10.1002/wdev.87
 1149 Schmid, T., & Hajnal, A. (2015). Signal transduction during *C. elegans* vulval development: a NeverEnding
 1150 story. *Curr Opin Genet Dev*, 32, 1-9. doi:10.1016/j.gde.2015.01.006
 1151 Schwartz, M. L., & Jorgensen, E. M. (2016). SapTrap, a Toolkit for High-Throughput CRISPR/Cas9 Gene
 1152 Modification in *Caenorhabditis elegans*. *Genetics*, 202(4), 1277-1288.
 1153 doi:10.1534/genetics.115.184275
 1154 Seydoux, G., Savage, C., & Greenwald, I. (1993). Isolation and characterization of mutations causing
 1155 abnormal eversion of the vulva in *Caenorhabditis elegans*. *Dev Biol*, 157(2), 423-436.
 1156 doi:10.1006/dbio.1993.1146
 1157 Sharma-Kishore, R., White, J. G., Southgate, E., & Podbilewicz, B. (1999). Formation of the vulva in
 1158 *Caenorhabditis elegans*: a paradigm for organogenesis. *Development*, 126(4), 691-699.
 1159 Shemer, G., Kishore, R., & Podbilewicz, B. (2000). Ring formation drives invagination of the vulva in
 1160 *Caenorhabditis elegans*: Ras, cell fusion, and cell migration determine structural fates. *Dev Biol*,
 1161 221(1), 233-248. doi:10.1006/dbio.2000.9657
 1162 Shephard, F., Adenle, A. A., Jacobson, L. A., & Szewczyk, N. J. (2011). Identification and functional
 1163 clustering of genes regulating muscle protein degradation from amongst the known *C. elegans*
 1164 muscle mutants. *PLoS One*, 6(9), e24686. doi:10.1371/journal.pone.0024686
 1165 Sherwood, D. R., & Sternberg, P. W. (2003). Anchor cell invasion into the vulval epithelium in *C. elegans*.
 1166 *Dev Cell*, 5(1), 21-31. doi:10.1016/s1534-5807(03)00168-0
 1167 Simmer, F., Moorman, C., van der Linden, A. M., Kuijk, E., van den Berghe, P. V., Kamath, R. S., . . .
 1168 Plasterk, R. H. (2003). Genome-wide RNAi of *C. elegans* using the hypersensitive rrf-3 strain
 1169 reveals novel gene functions. *PLoS Biol*, 1(1), E12. doi:10.1371/journal.pbio.0000012
 1170 Soulavie, F., Hall, D. H., & Sundaram, M. V. (2018). The AFF-1 exoplasmic fusogen is required for
 1171 endocytic scission and seamless tube elongation. *Nat Commun*, 9(1), 1741. doi:10.1038/s41467-
 1172 018-04091-1
 1173 Sternberg, P. W., & Horvitz, H. R. (1989). The combined action of two intercellular signaling pathways
 1174 specifies three cell fates during vulval induction in *C. elegans*. *Cell*, 58(4), 679-693.
 1175 doi:10.1016/0092-8674(89)90103-7
 1176 Strilić, B., Kucera, T., Eglinger, J., Hughes, M. R., McNagny, K. M., Tsukita, S., . . . Lammert, E. (2009). The
 1177 molecular basis of vascular lumen formation in the developing mouse aorta. *Dev Cell*, 17(4), 505-
 1178 515. doi:10.1016/j.devcel.2009.08.011
 1179 Sulston, J. E., & Horvitz, H. R. (1977). Post-embryonic cell lineages of the nematode, *Caenorhabditis*
 1180 *elegans*. *Dev Biol*, 56(1), 110-156. doi:10.1016/0012-1606(77)90158-0
 1181 Suman, S. K., Daday, C., Ferraro, T., Vuong-Brender, T., Tak, S., Quintin, S., . . . Labouesse, M. (2019). The
 1182 plakin domain of *C. elegans* VAB-10/plectin acts as a hub in a mechanotransduction pathway to
 1183 promote morphogenesis. *Development*, 146(24). doi:10.1242/dev.183780
 1184 Suzuki, N., Toyoda, H., Sano, M., & Nishiwaki, K. (2006). Chondroitin acts in the guidance of gonadal
 1185 distal tip cells in *C. elegans*. *Dev Biol*, 300(2), 635-646. doi:10.1016/j.ydbio.2006.08.037

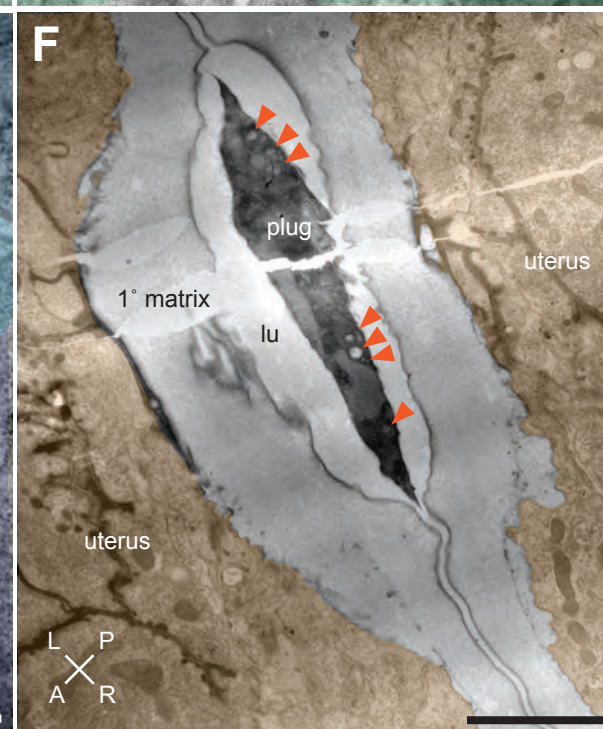
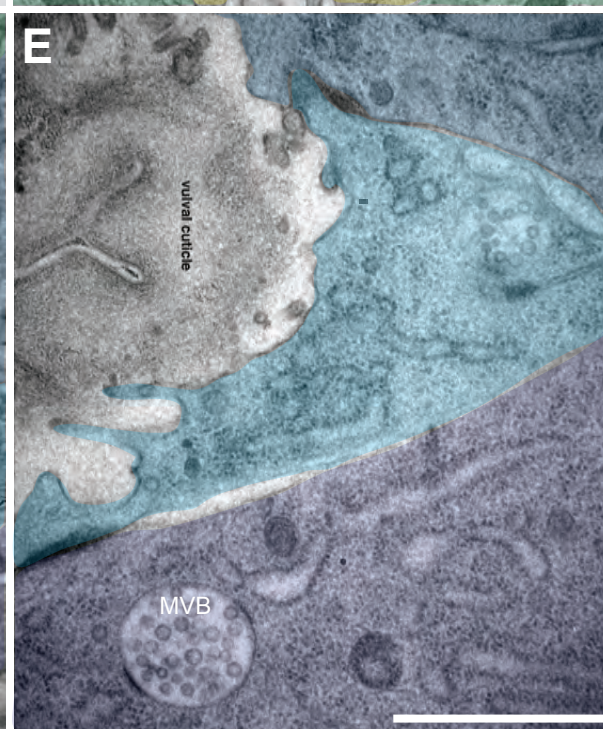
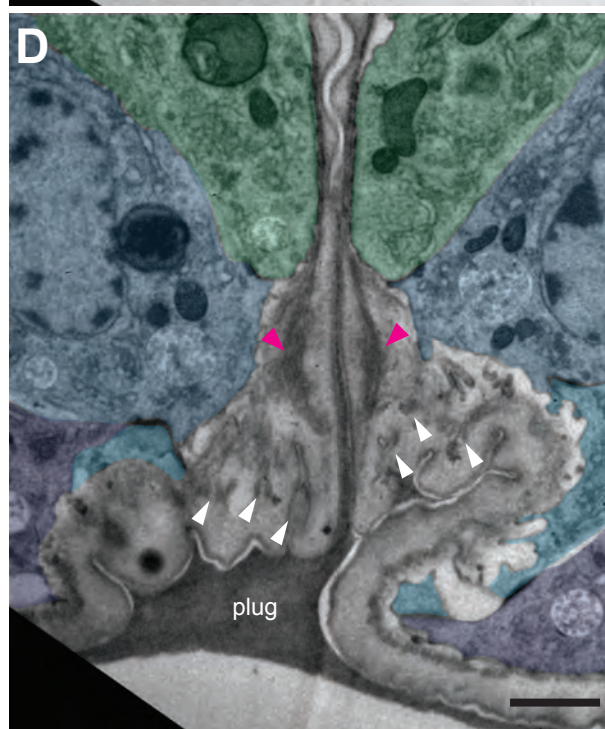
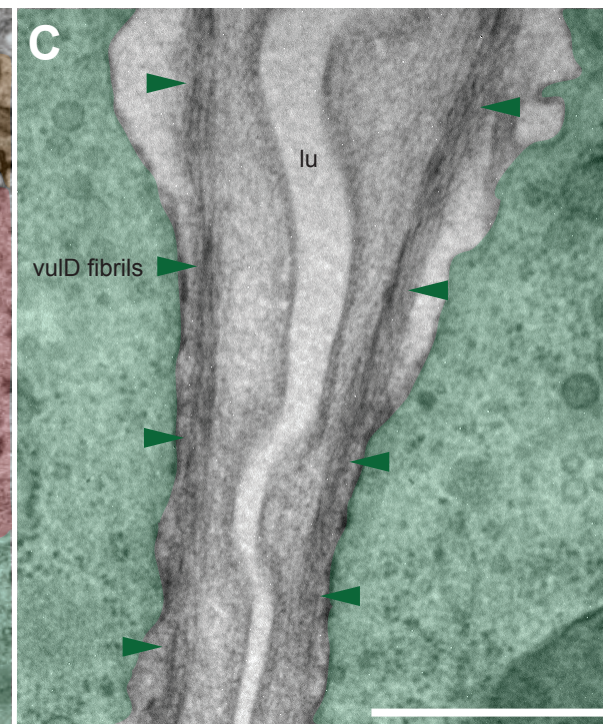
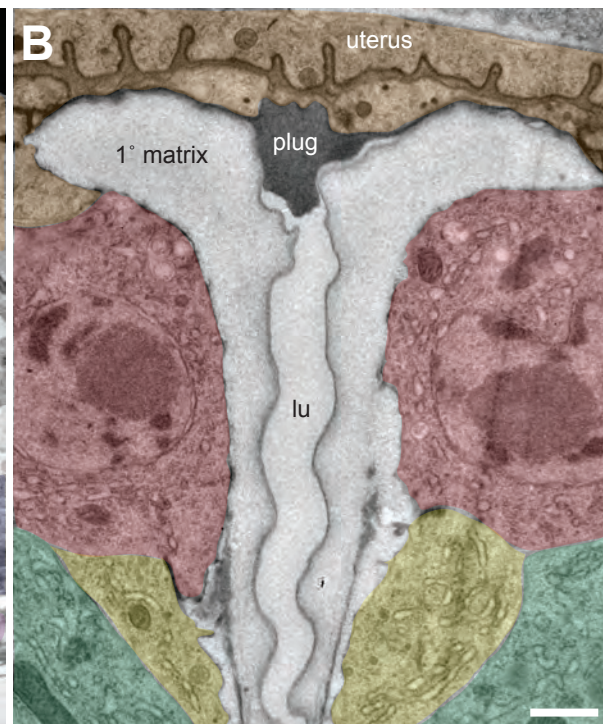
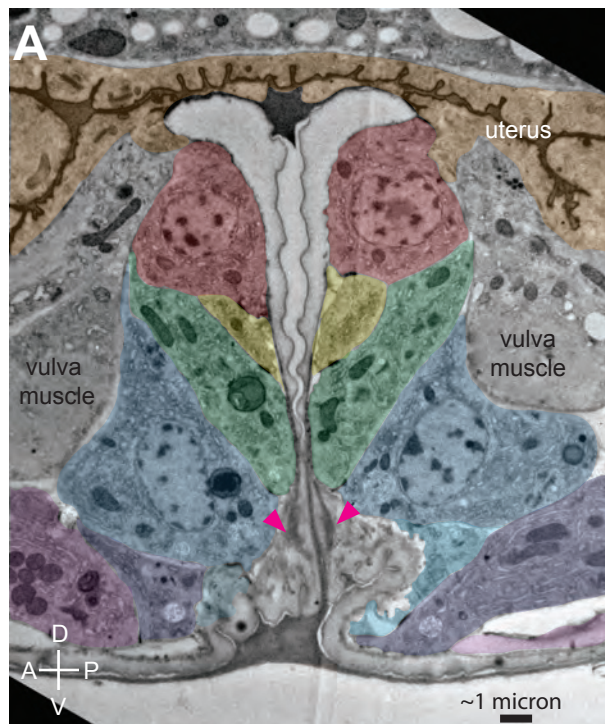
- Syed, Z. A., Bougé, A. L., Byri, S., Chavoshi, T. M., Tång, E., Bouhin, H., . . . Uv, A. (2012). A luminal glycoprotein drives dose-dependent diameter expansion of the *Drosophila melanogaster* hindgut tube. *PLoS Genet*, *8*(8), e1002850. doi:10.1371/journal.pgen.1002850
- Tønning, A., Hemphälä, J., Tång, E., Nannmark, U., Samakovlis, C., & Uv, A. (2005). A transient luminal chitinous matrix is required to model epithelial tube diameter in the *Drosophila* trachea. *Dev Cell*, *9*(3), 423-430. doi:10.1016/j.devcel.2005.07.012
- Vuong-Brender, T. T. K., Suman, S. K., & Labouesse, M. (2017). The apical ECM preserves embryonic integrity and distributes mechanical stress during morphogenesis. *Development*, *144*(23), 4336-4349. doi:10.1242/dev.150383
- Webster, M. J., & Tarran, R. (2018). Slippery When Wet: Airway Surface Liquid Homeostasis and Mucus Hydration. *Curr Top Membr*, *81*, 293-335. doi:10.1016/bs.ctm.2018.08.004
- Weimer, R. M. (2006). Preservation of *C. elegans* tissue via high-pressure freezing and freeze-substitution for ultrastructural analysis and immunocytochemistry. *Methods Mol Biol*, *351*, 203-221. doi:10.1385/1-59745-151-7:203
- Yang, Q., Roiz, D., Mereu, L., Daube, M., & Hajnal, A. (2017). The Invading Anchor Cell Induces Lateral Membrane Constriction during Vulval Lumen Morphogenesis in *C. elegans*. *Dev Cell*, *42*(3), 271-285.e273. doi:10.1016/j.devcel.2017.07.008
- Yang, Y., Zhang, Y., Li, W. J., Jiang, Y., Zhu, Z., Hu, H., . . . Ou, G. (2017). Spectraplakins Induce Positive Feedback between Fusogens and the Actin Cytoskeleton to Promote Cell-Cell Fusion. *Dev Cell*, *41*(1), 107-120.e104. doi:10.1016/j.devcel.2017.03.006

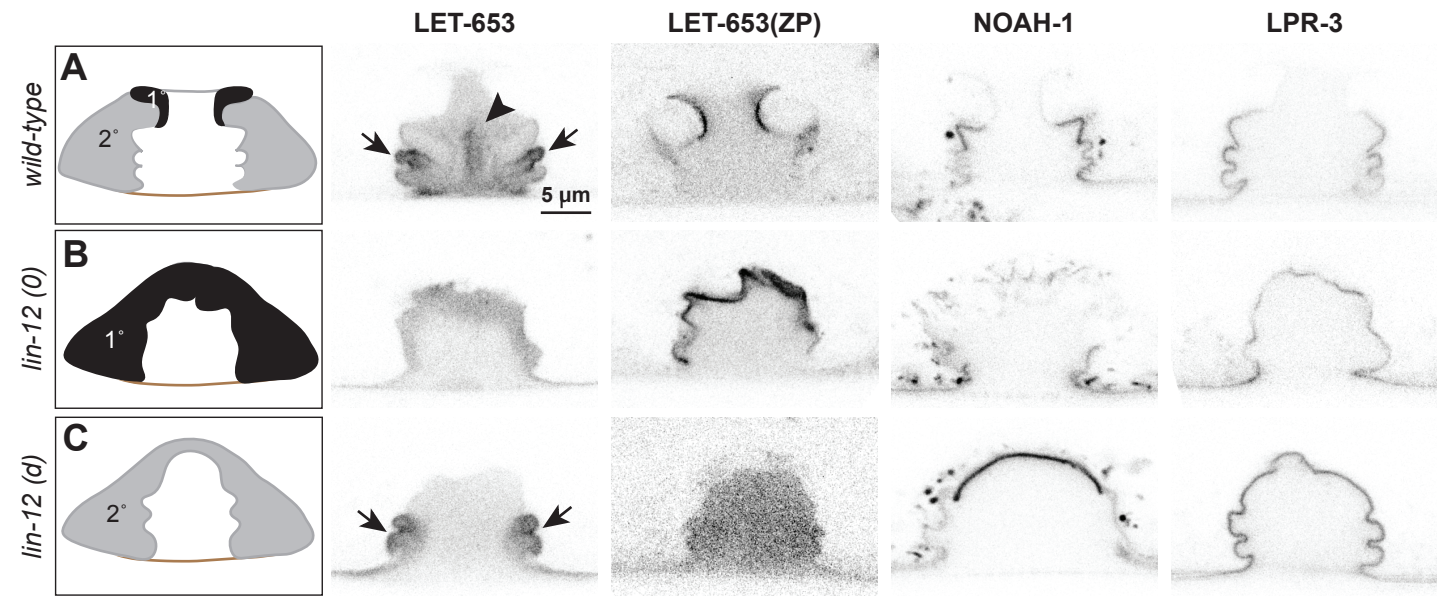


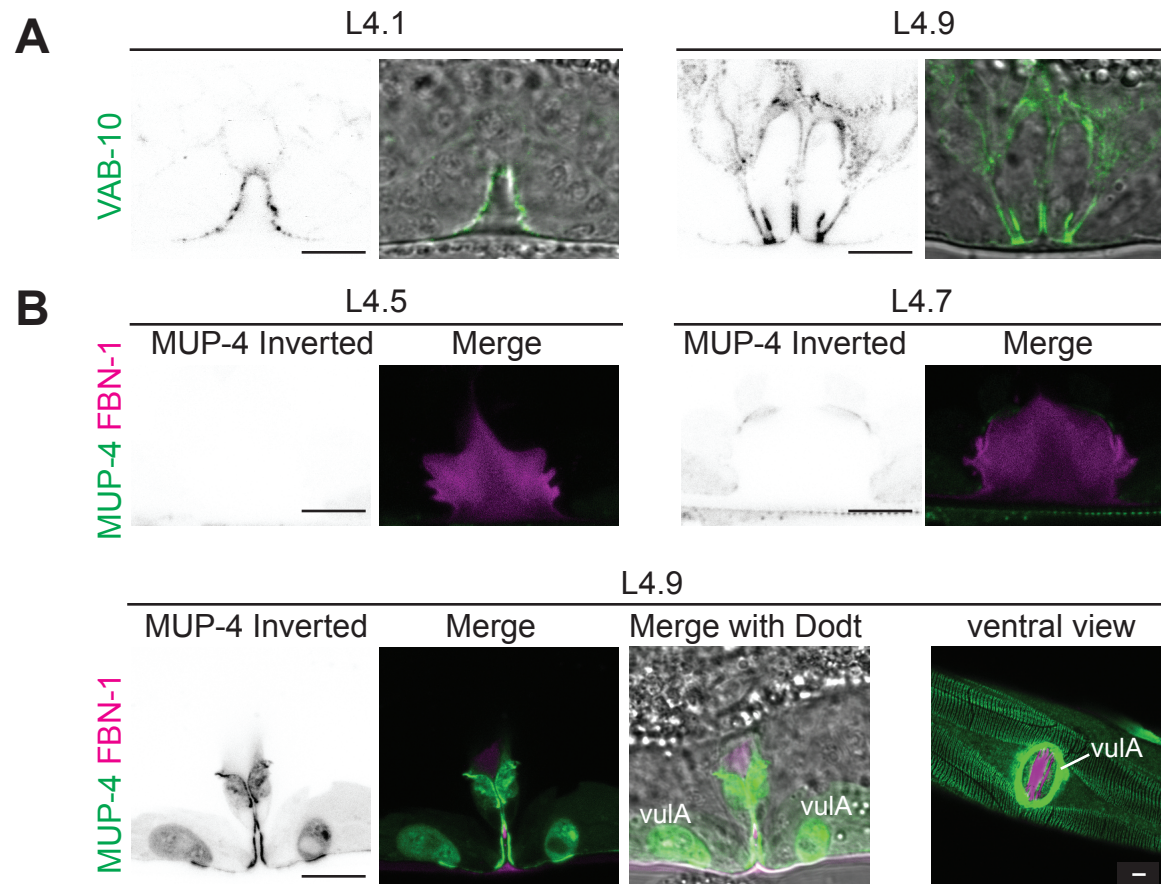


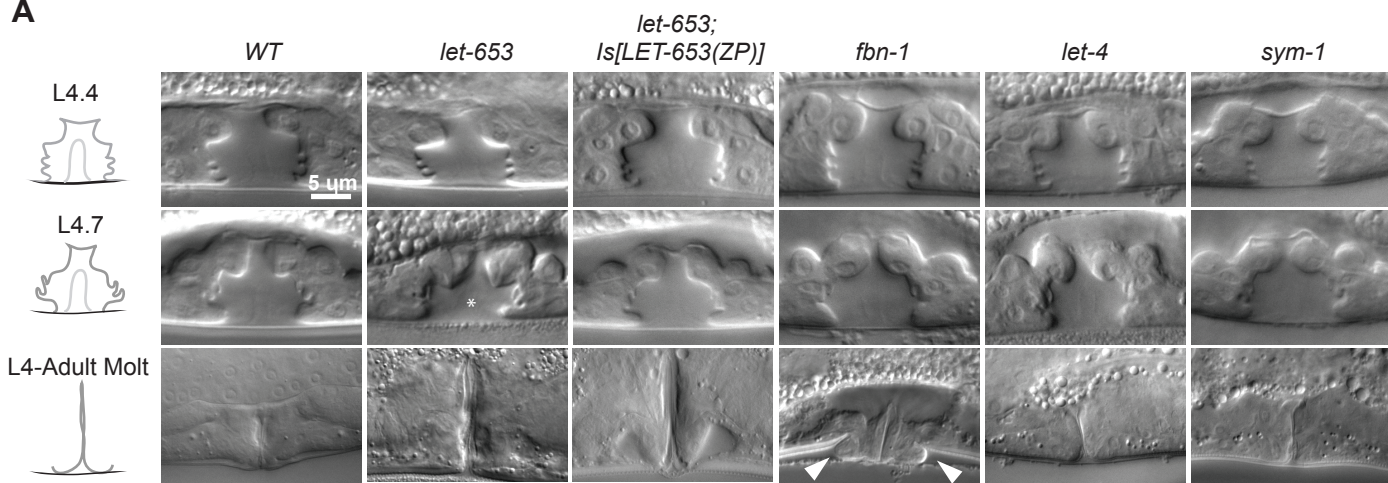
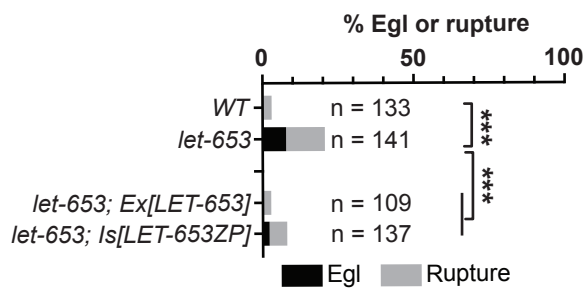
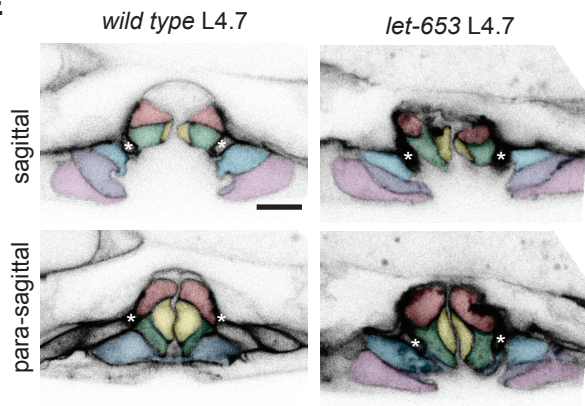
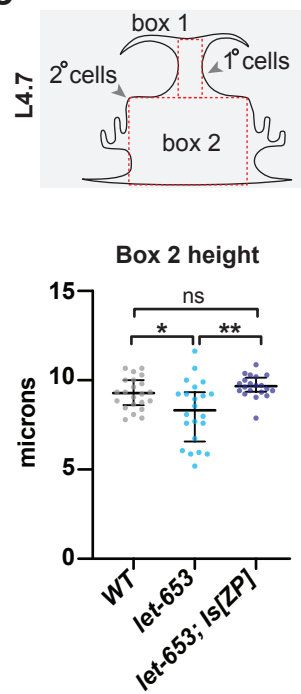
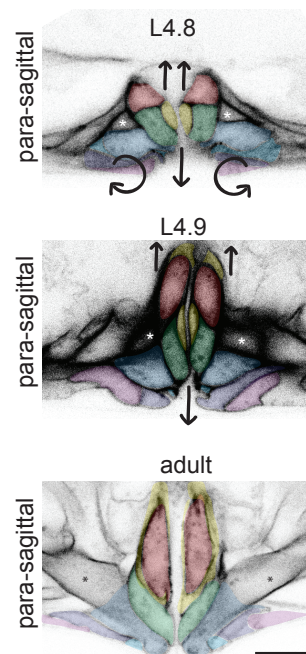
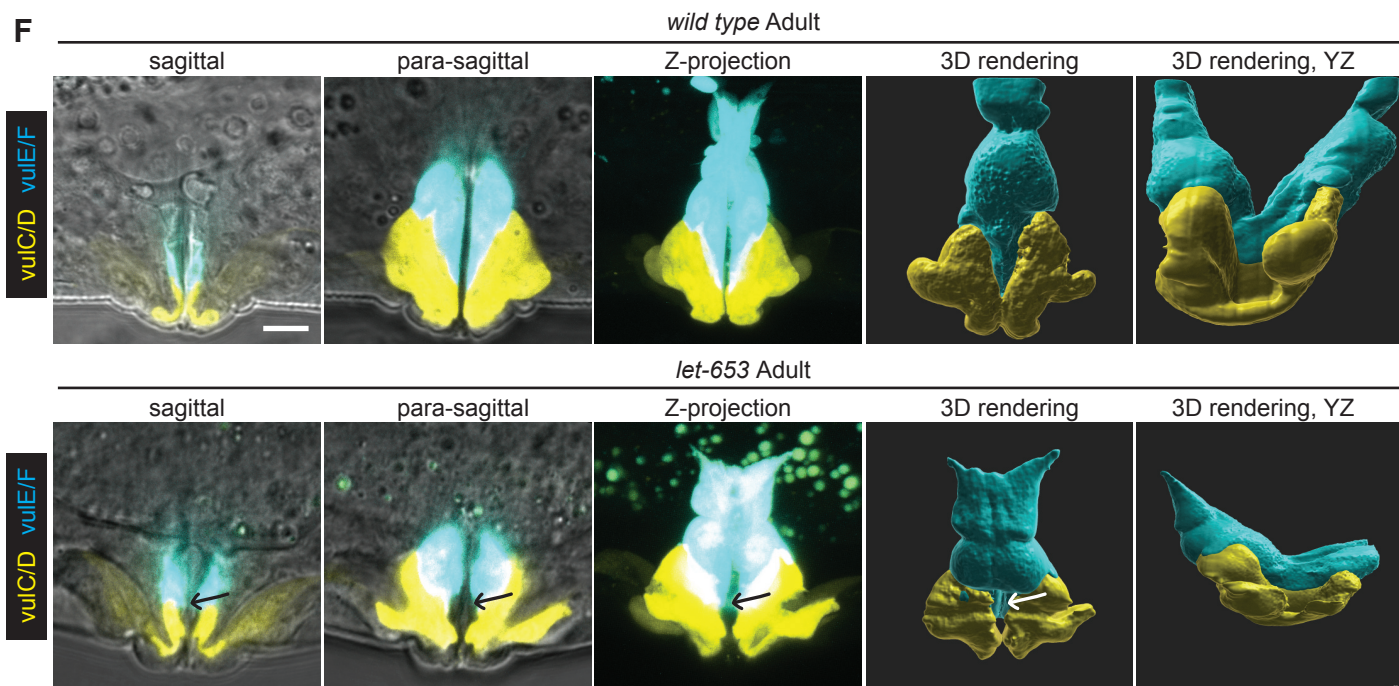


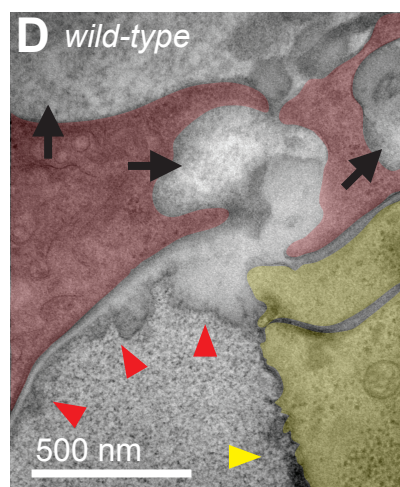
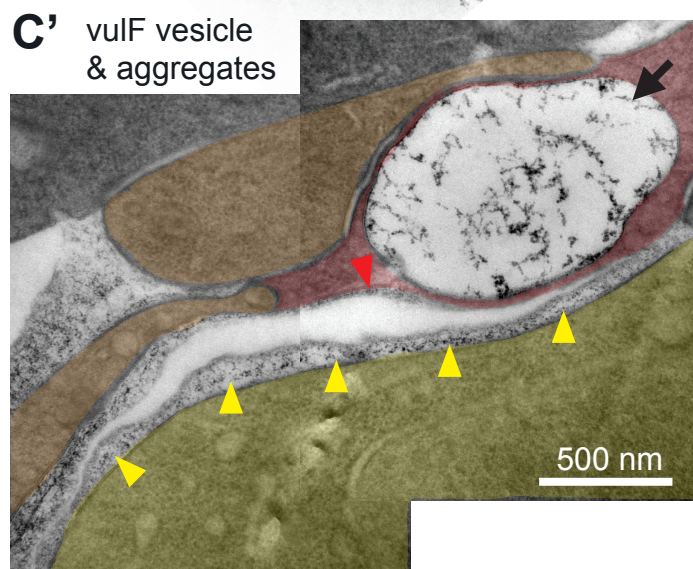
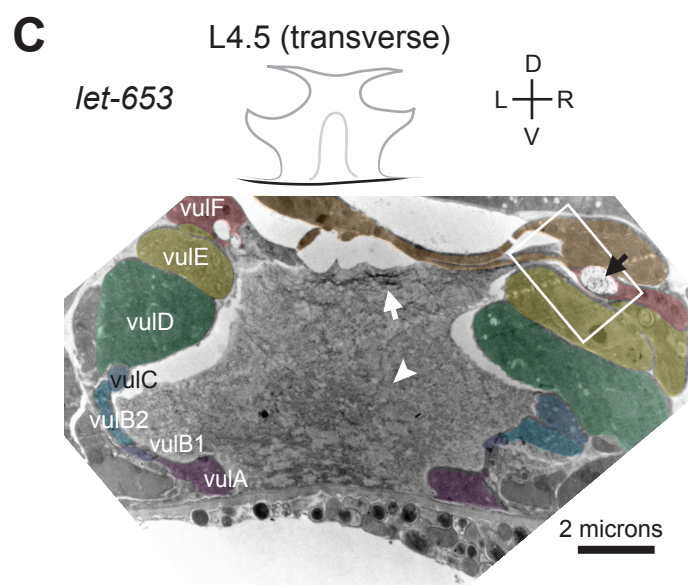
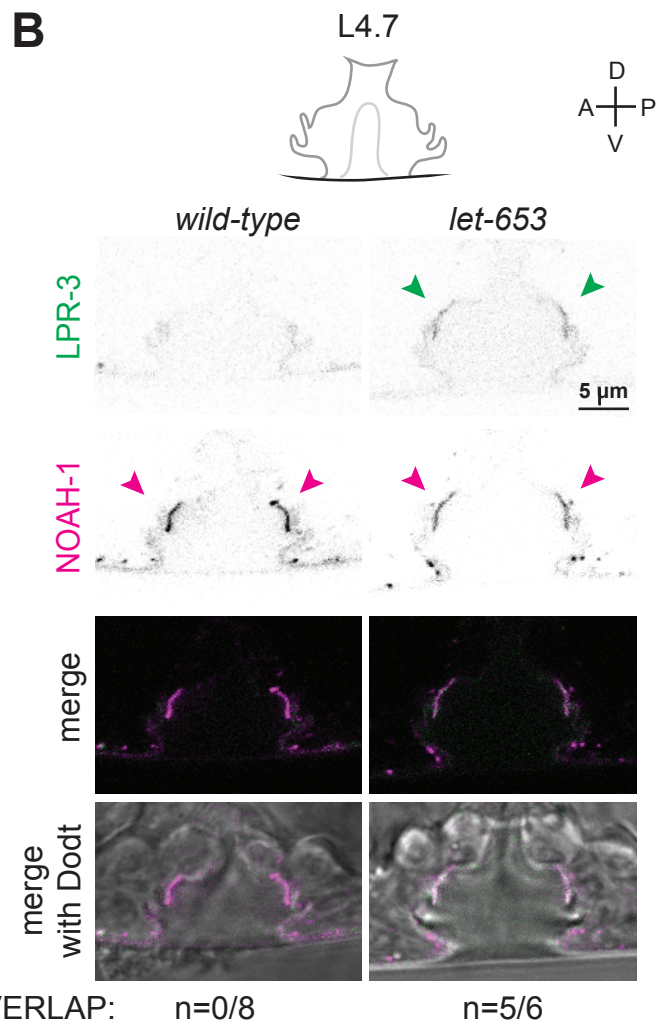
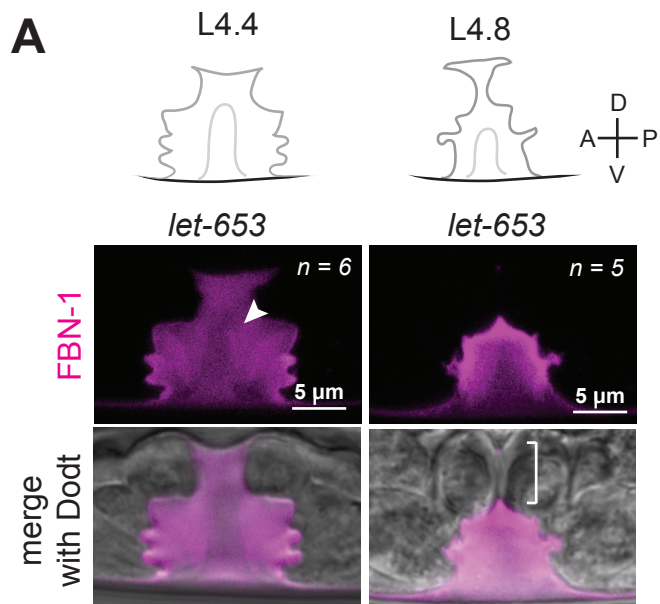


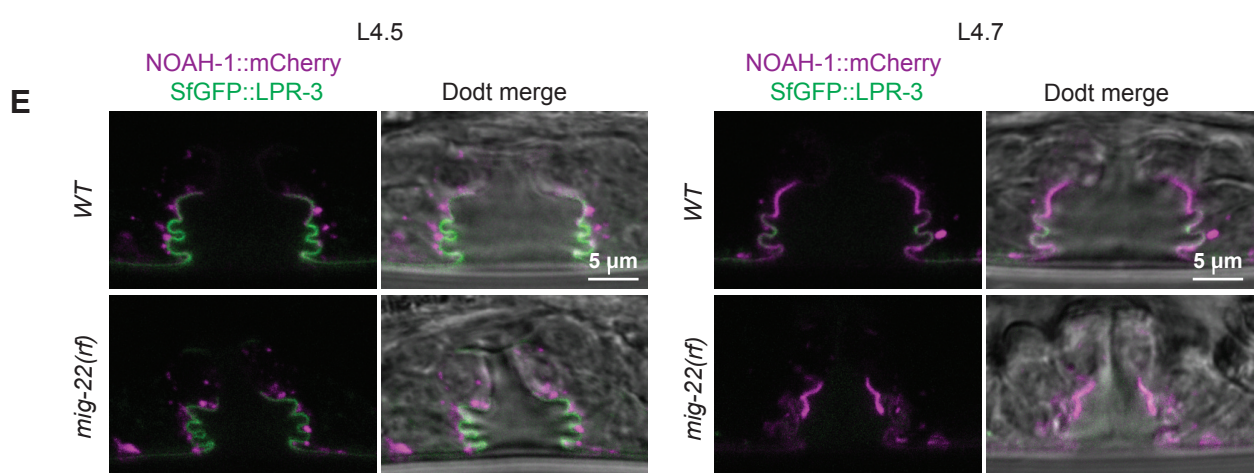
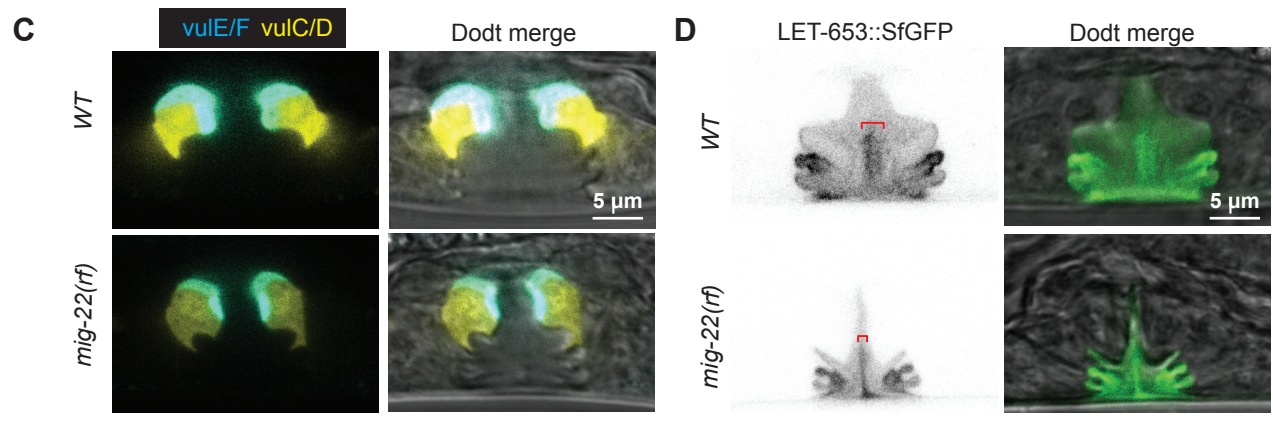
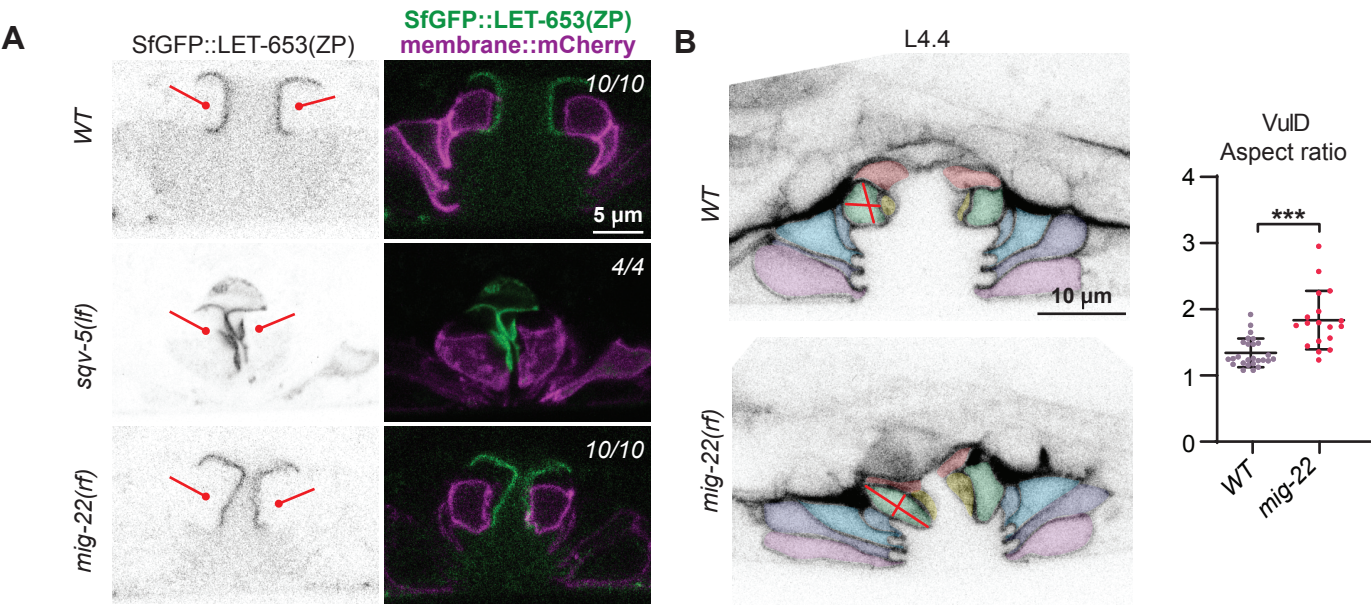


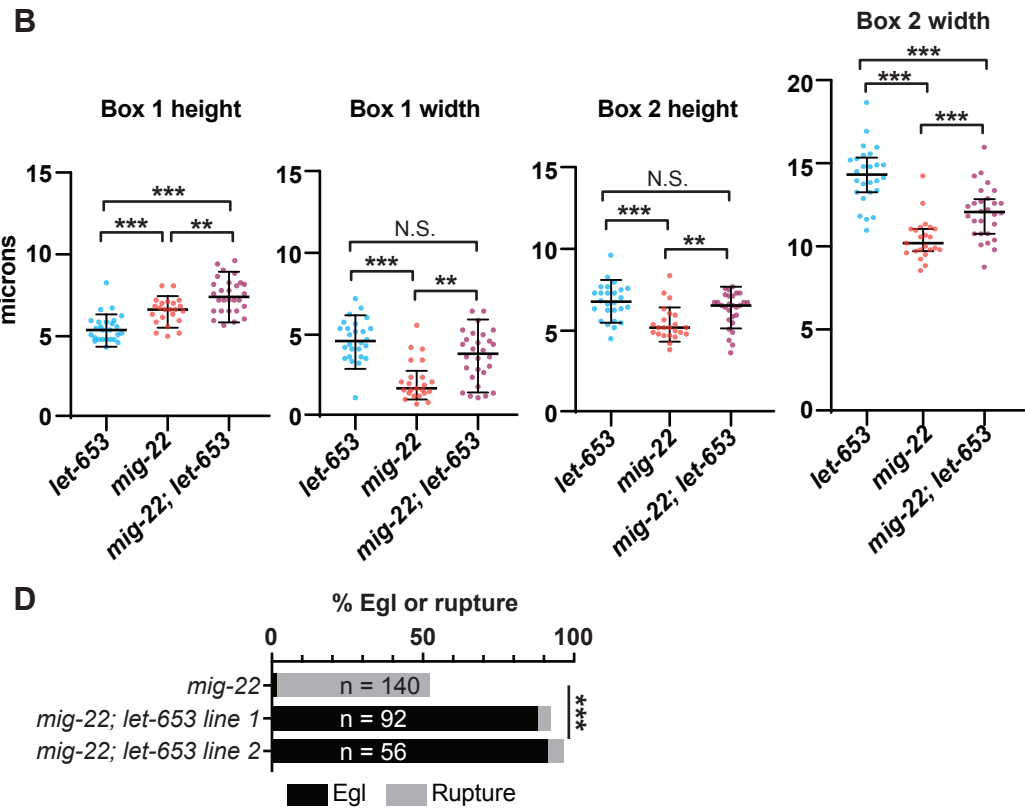
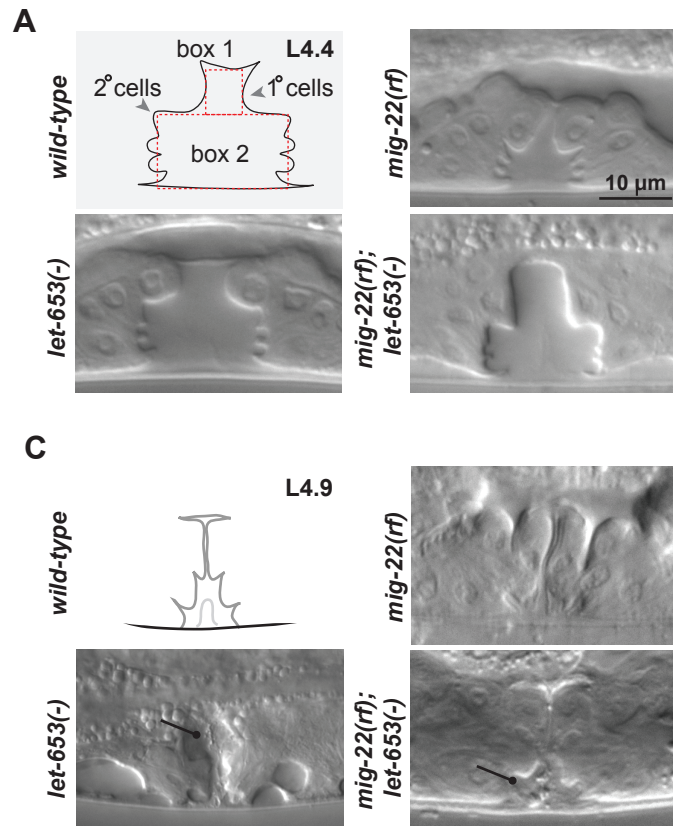




A**B****E****C****D wild type vulva eversion****F**



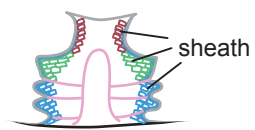




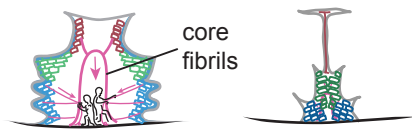
A lumen
inflation



B membrane
stabilization

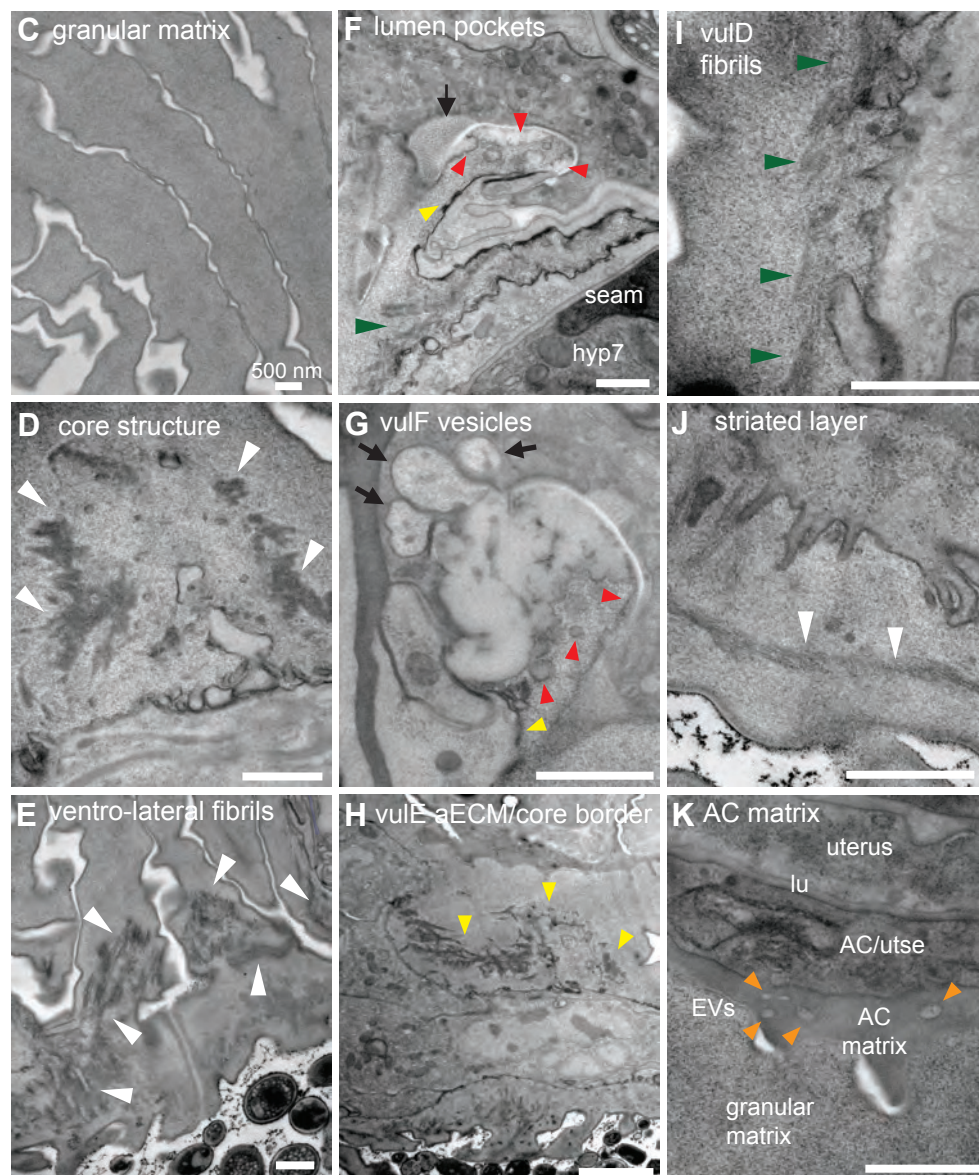
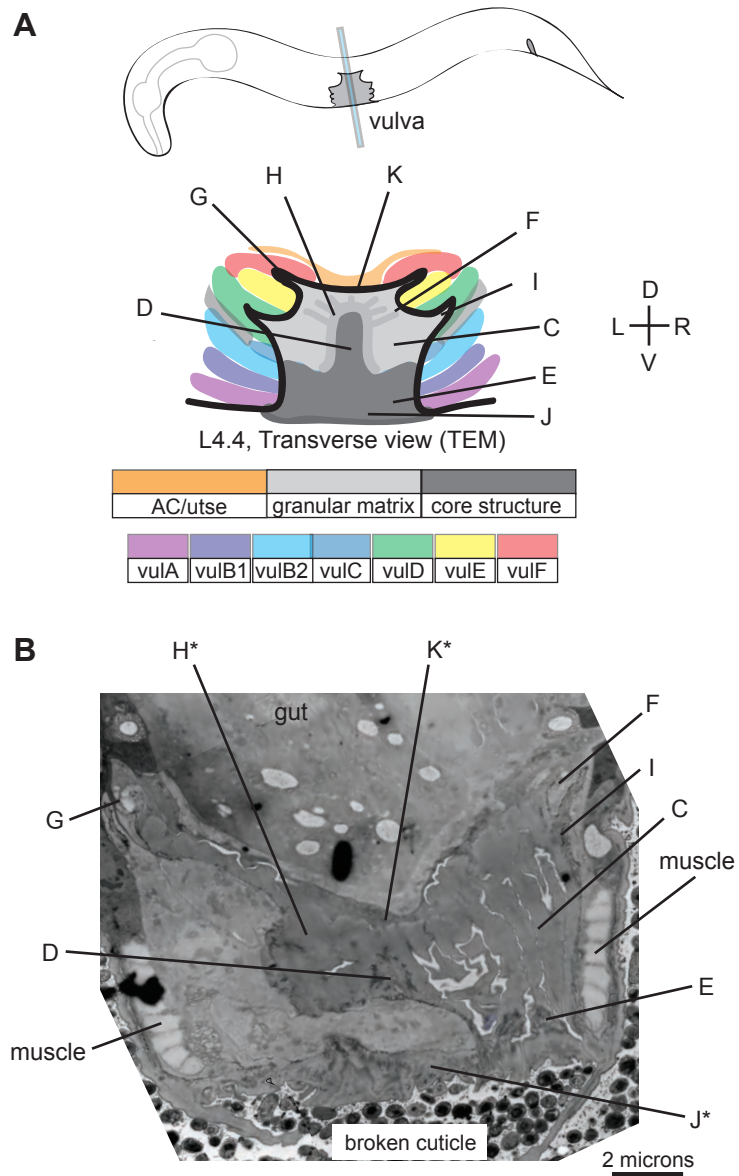


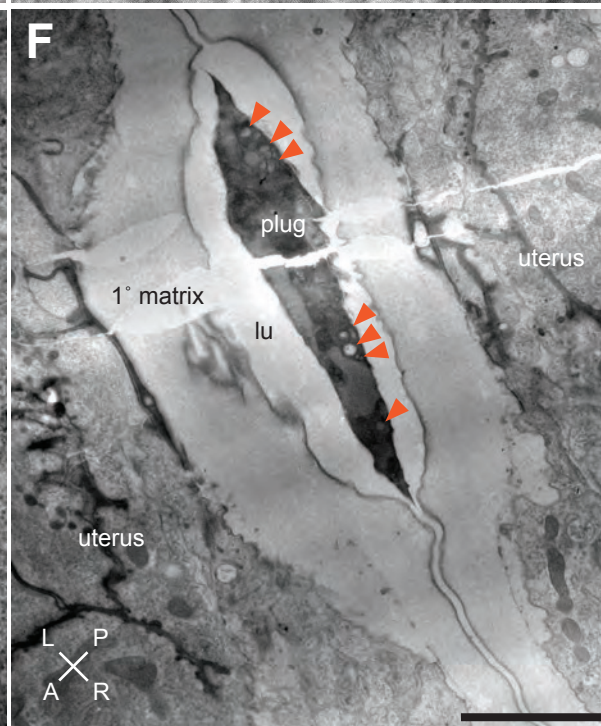
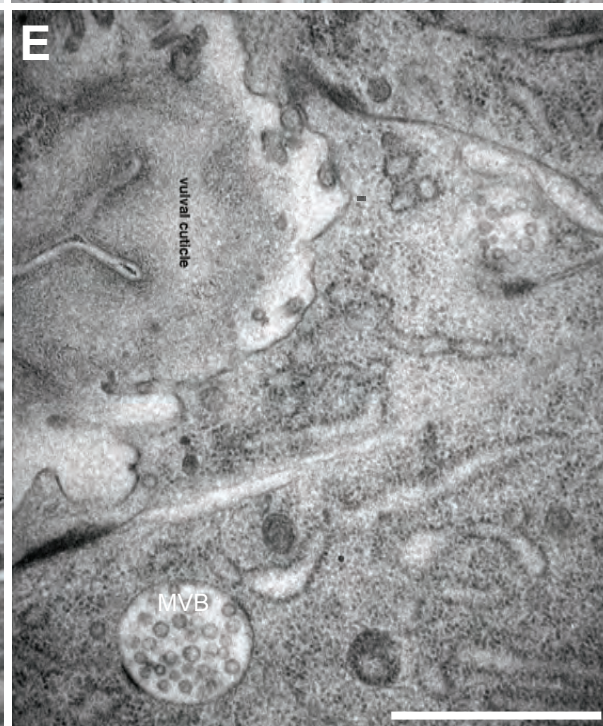
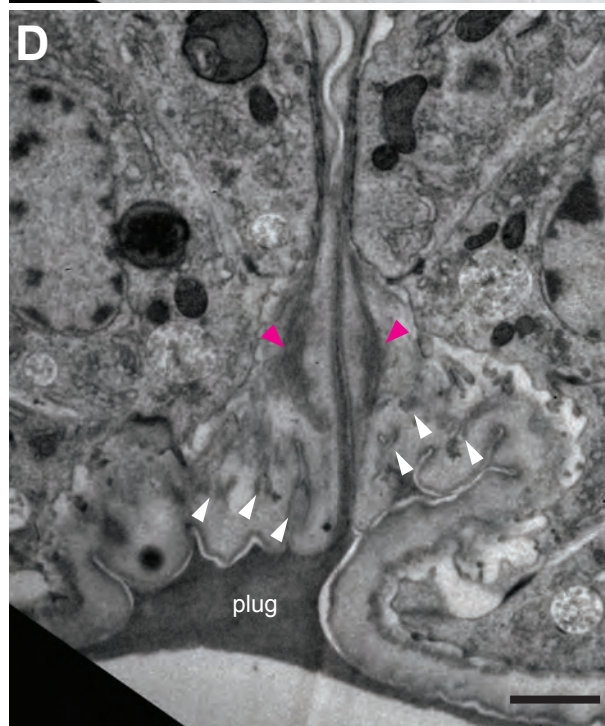
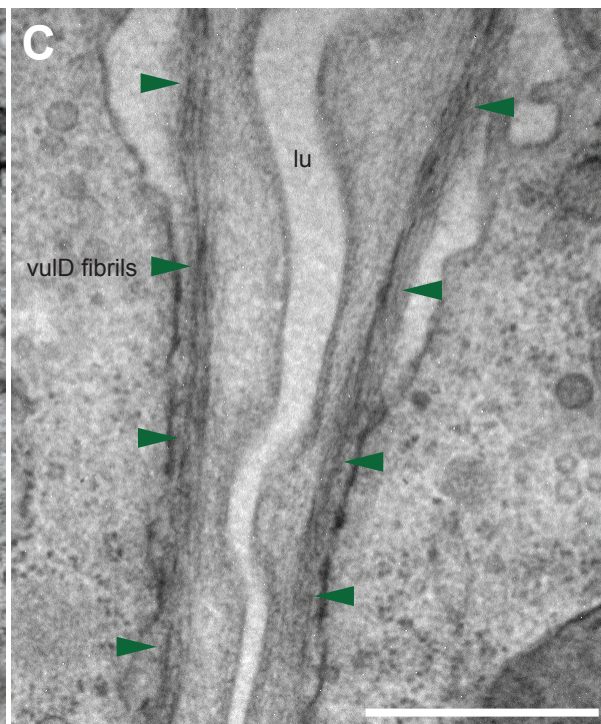
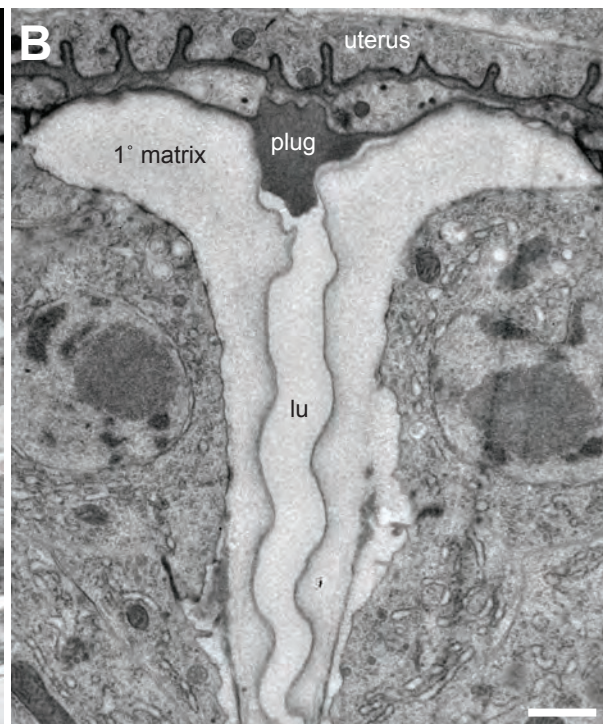
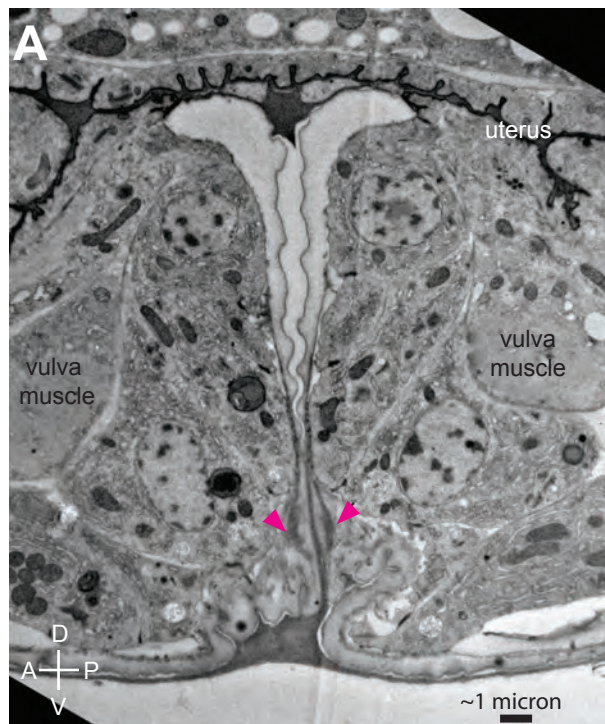
C lumen
closure



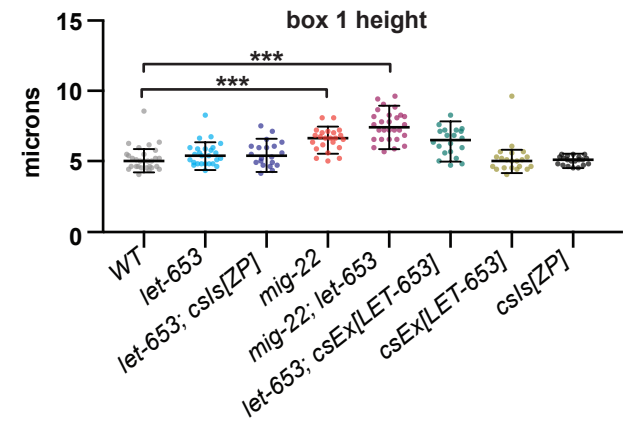
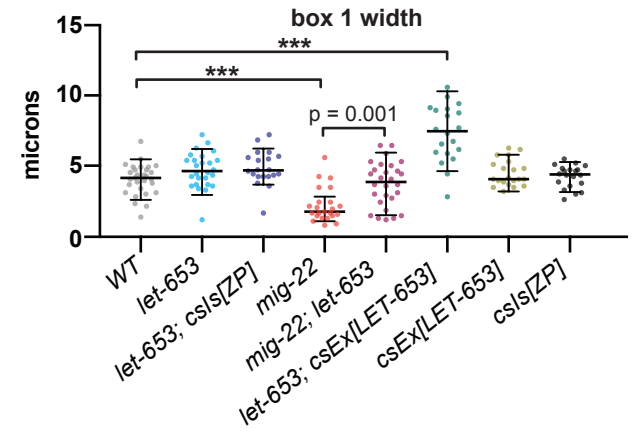
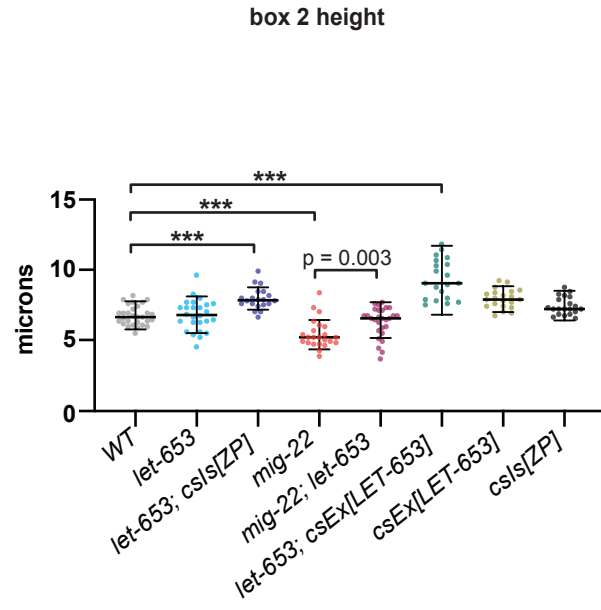
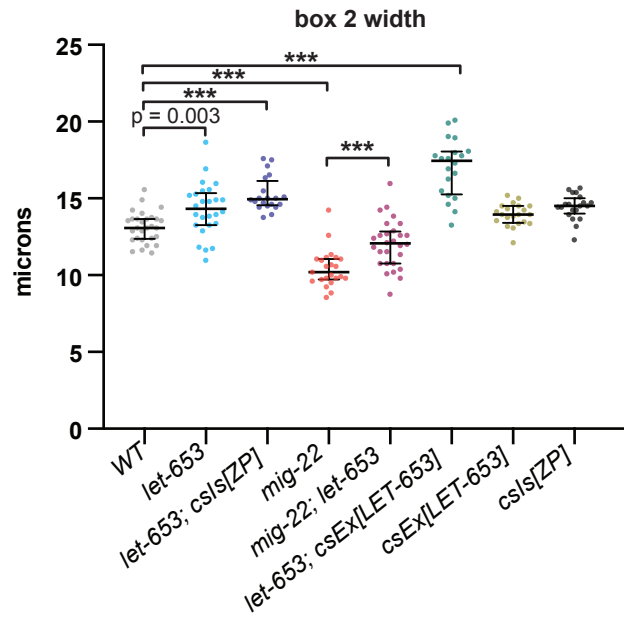
D cuticle-lined
mature tube



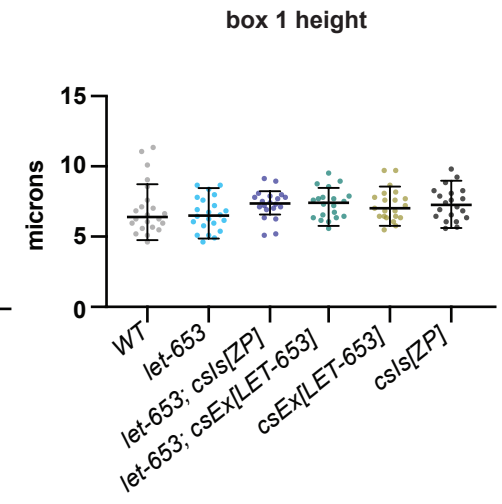
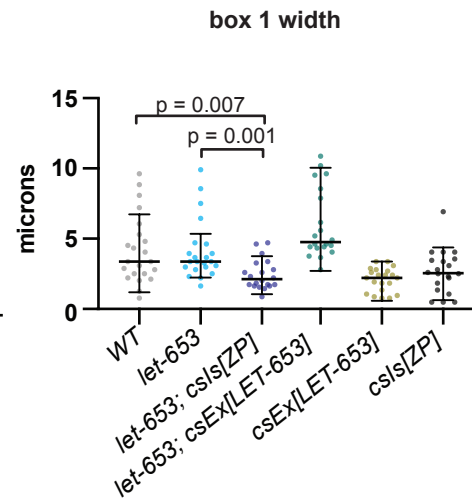
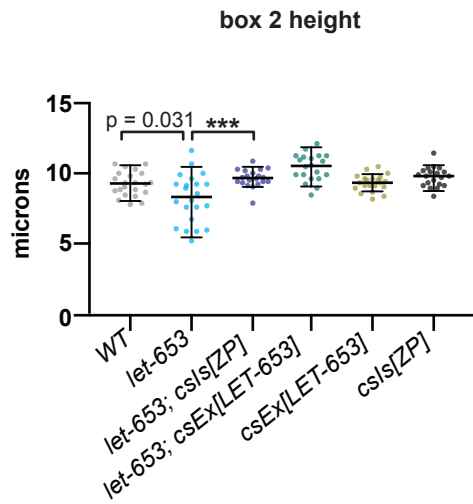
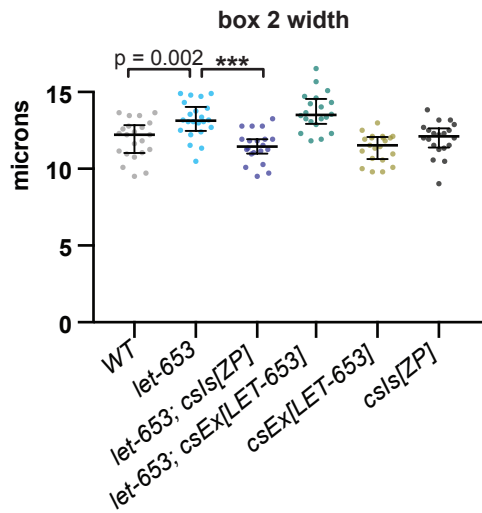




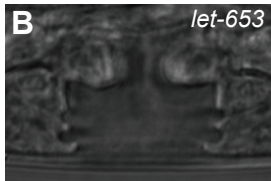
L4.4 measurements



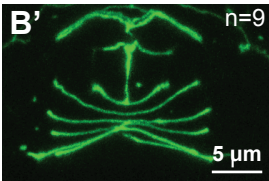
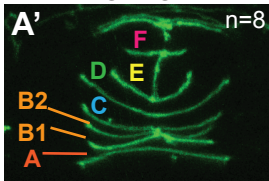
L4.7 measurements



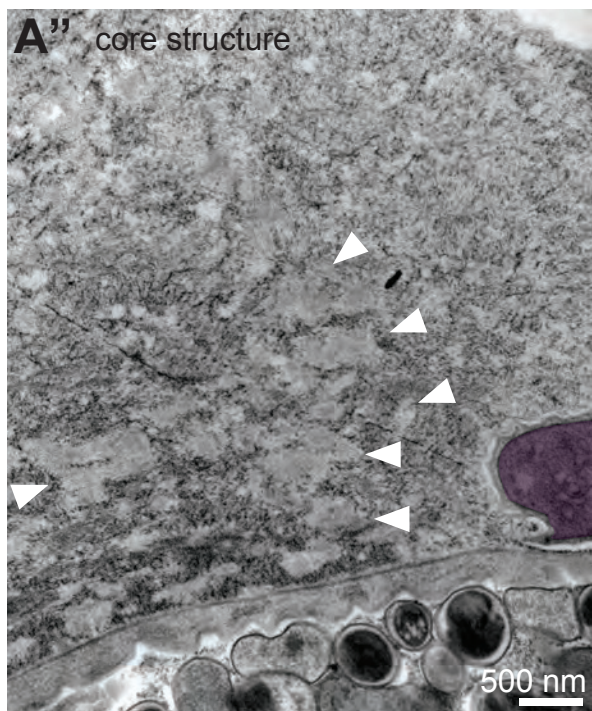
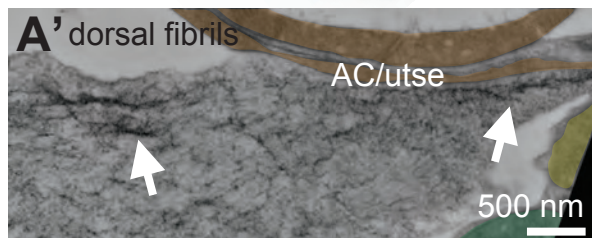
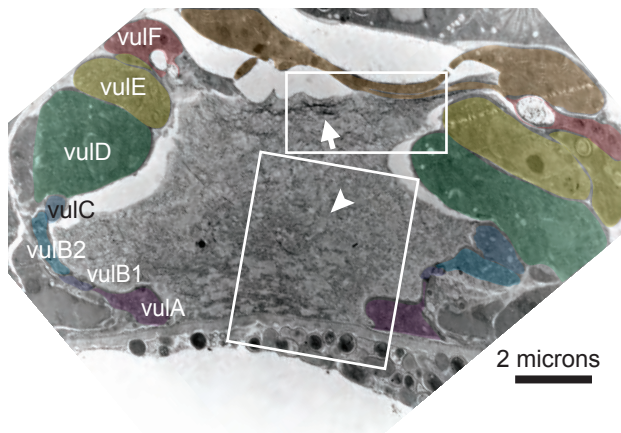
Dodt



DLG-1::GFP



A *let-653* (from Fig. 9)



B *wild-type* (from Fig. 4)

